

# Electronic states, Mott localization, electron-lattice coupling, and dimerization for correlated one-dimensional systems. II.

Adam Rycerz and Jozef Spałek,  
 Marian Smoluchowski Institute of Physics, Jagiellonian University,  
 ulica Reymonta 4, 30-059 Kraków, Poland

We discuss physical properties of strongly correlated electron states for a linear chain obtained with the help of the recently proposed new method combining the exact diagonalization in the Fock space with an *ab initio* readjustment of the single-particle orbitals in the correlated state. The method extends the current discussion of the correlated states since the properties are obtained with varying lattice spacing. The finite system of  $N$  atoms *evolves* with the increasing interatomic distance from a Fermi-liquid-like state into the Mott insulator. The criteria of the localization are discussed in detail since the results are already convergent for  $N \geq 8$ . During this process the Fermi-Dirac distribution gets smeared out, the effective band mass increases by  $\sim 50\%$ , and the spin-spin correlation functions reduce to those for the Heisenberg antiferromagnet. Values of the microscopic parameters such as the hopping and the kinetic-exchange integrals, as well as the magnitude of both intra- and inter-atomic Coulomb and exchange interactions are calculated. We also determine the values of various local electron-lattice couplings and show that they are *comparable* to the kinetic exchange contribution in the strong-correlation limit. The magnitudes of the dimerization and the zero-point motion are also discussed. Our results provide a canonical example of a tractable strongly correlated system with a precise, first-principle description as a function of interatomic distance of a model system involving *all* hopping integrals, *all* pair-site interactions, and the *exact* one-band Wannier functions.

PACS Nos. 71.10.Hf, 71.27.+a, 71.30.th

## I. INTRODUCTION

In spite of the enormous successes of the approach based on the effective single-particle wave equation<sup>1</sup> for many 3-dimensional metals and semiconductors, the understanding of the so-called *correlated fermionic systems* is still lacking, particularly for the systems of lower dimensionality,  $d = 1$  and 2. This is because in their description of the electronic states the role of the long-range Coulomb interaction is crucial, as the charge screening becomes less effective<sup>2</sup>. In result, the interaction cannot be regarded as small and phenomena such as the spin-charge separation<sup>3</sup>, the Mott metal-insulator transition<sup>4</sup> or the strong electron-lattice interaction (leading among others to the Peierls distorted<sup>5</sup> state) appear in various quasi-one-dimensional systems. In addition, a normal metallic state in quantum wires<sup>6</sup> and nanotubes<sup>7</sup>, as well as the superconducting state in organic 1d metals are also observed, raising the question about the relative role of the single-particle dynamics and the repulsive Coulomb interactions treated in a nonperturbational manner. To phrase it differently, in one-dimensional systems we consider here the single-particle states and the Coulomb interactions are treated on equal footing from the outset.

We have recently proposed<sup>8,9</sup> (those References are regarded as Part I) a new approach to the correlated fermion systems, which provides rigorous results for model (one-band) systems containing  $N \leq 12$  atoms. The results concerning the principal local characteristics are very rapidly converging and provide a reliable estimate of the system characteristics such as the micro-

scopic interaction parameters, the ground state energy, the magnitude of Peierls distortion or the zero point motion, all as function of the interatomic distance. It is the purpose of this paper to provide a complete picture of the electronic and lattice properties by providing the band effective masses, the magnitude of exchange interactions and related to them the spin-spin correlation functions, the detailed discussion of a gradual transition from a metal to the Mott insulator, and the constants of the local coupling of electrons to the lattice. We also consider the dimerized state of the system. We believe that analysis of this type containing a combination of a rigorous treatment of the interactions in the Fock space combined with *ab initio* treatment of the single-particle wave-functions in the Hilbert state, that are allowed to relax in the correlated state, provides the first step in a rigorous quantitative analysis of linear-chain of finite size and *correlated* quantum dot systems. In other words, our first-principle method is specifically designed to treat such correlated systems, although some general conclusions are also discussed.

The structure of the paper is as follows. In the next section (and in Appendix A) we summarize our method and provide the details not published before. In Section III the crossover from metallic to the Mott insulating state is dealt with to provide the proper ground state for a subsequent analysis. In Section IV we discuss the magnetic (kinetic-exchange) interactions and the spin-spin correlation functions. In Section V we determine the local electron-phonon coupling constants and compare their magnitude with that of the magnetic interactions.

The main feature of the above analysis is to provide the properties as a function of the lattice spacing. In this respect our approach differs from the numerous solutions<sup>2-4</sup> of parametrized models such as the (extended) Hubbard model, where the physical properties are discussed as a function of the model parameters. Here *all* one- and two-site parameters are calculated explicitly and this feature allows for a consideration of e.g. one-band system with inclusion of both the *exact* Wannier functions, *all* hopping integrals and *all* two-site interactions.

## II. METHOD

We start with the Hamiltonian containing  $N$  lattice sites with *all* hopping integrals  $t_{ij}$  and with *all* two-site interactions, which for the linear chain with periodic boundary conditions can be written as

$$\begin{aligned} \mathcal{H} = \sum_{i=0}^{N-1} \left\{ \epsilon_a n_i + U n_{i\uparrow} n_{i\downarrow} + \sum_{j=0}^{i-1} \left[ \left( K_{ij} - \frac{1}{2} J_{ij} \right) n_i n_j \right. \right. \\ \left. \left. - 2 J_{ij} \mathbf{S}_i \cdot \mathbf{S}_j + \sum_{\sigma} (t_{ij} + V_{ij}(n_{i\sigma} + n_{j\sigma})) (a_{i\sigma}^{\dagger} a_{j\sigma} + \text{h.c.}) \right. \right. \\ \left. \left. + J_{ij} (a_{i\uparrow}^{\dagger} a_{i\downarrow}^{\dagger} a_{j\downarrow} a_{j\uparrow} + \text{h.c.}) \right] \right\}. \end{aligned} \quad (1)$$

The first term represents the atomic energy (we include it explicitly, since  $\epsilon_a$  changes with the varying lattice constant). The second describes the intraatomic Coulomb interaction (the Hubbard term). The next two terms represent the direct intersite Coulomb interaction ( $\sim K_{ij}$ ) and the Heisenberg-Dirac exchange ( $\sim J_{ij}$ ). The fifth and the sixth term express respectively the single-particle ( $\sim t_{ij}$ ) and the correlated-hopping ( $\sim V_{ij}$ ) terms, whereas the last includes the pair-electron hopping  $i \rightleftharpoons j$ . The microscopic parameters have been defined before (cf. Appendix B of Ref.<sup>8</sup>). Their values as a function of the interatomic distance  $R$  have been determined before<sup>9</sup>; here we provide in Table I the values of the interaction parameters together with their asymptotic analytic expressions, which reproduce well their values for  $R \gtrsim 4a_0$  ( $\gtrsim 2\text{\AA}$ ).

One should underline that the parameters are here defined in terms of exact Wannier function for this one-band (one-orbital-per-site) system, that is defined as

$$w_i(\mathbf{r}) = \sum_{j=1}^N \beta_{i-j} \Psi_j(\mathbf{r}), \quad (2)$$

where  $\Psi_j(\mathbf{r})$  represents atomic function of  $s$ -type centered on site  $j$ :

$$\Psi_j(\mathbf{r}) \equiv \Psi(\mathbf{r} - \mathbf{R}_j) = \left( \frac{\alpha^3}{\pi} \right)^{1/2} \exp(-\alpha |\mathbf{r} - \mathbf{R}_j|). \quad (3)$$

The quantity  $\alpha$ , which represents the inverse orbital size (and calculated in units of the Bohr radius  $a_0$ ) will be determined by optimizing the orthonormal atomic (Wannier) basis in the correlated state. In effect, the parameters are  $\epsilon_a = \langle w_i | T | w_i \rangle$ ,  $t_{i-j} = \langle w_i | T | w_j \rangle$ ,  $U = \langle w_i w_i | V_{12} | w_i w_i \rangle$ ,  $K_{i-j} = \langle w_i w_j | V_{12} | w_i w_j \rangle$ ,  $J_{i-j} = \langle w_i w_j | V_{12} | w_j w_i \rangle = \langle w_i w_i | V_{12} | w_j w_j \rangle$ , and  $V_{i-j} = \langle w_i w_i | V_{12} | w_i w_j \rangle$ . The operator  $T$  represents the full single-particle lattice potential, i.e.

$$\begin{aligned} T(\mathbf{r}) = -\frac{\hbar^2}{2m} \nabla^2 - \sum_{j=0}^{N-1} \frac{e^2}{|\mathbf{r} - \mathbf{R}_j|} \\ \stackrel{\text{a.u.}}{=} -\frac{1}{2} \nabla^2 - \sum_{j=0}^{N-1} \frac{2}{|\mathbf{r} - \mathbf{R}_j|}, \end{aligned} \quad (4)$$

where a.u. means the expression in atomic units.  $V_{12} = e^2/|\mathbf{r}_1 - \mathbf{r}_2|$  is the usual Coulomb potential (we do not include any screening by e.g. core electrons as we want to discuss the model situation, but in a rigorous manner).

TABLE I. Microscopic parameters values for various interaction terms in the starting Hamiltonian for  $N = 8$  sites.

$R$ [ $a_0$ ]	$U$ [Ry]	$K_1$ [Ry]	$K_2$ [Ry]	$K_3$ [Ry]
2.0	2.301	1.077	0.676	0.450
2.5	1.949	0.843	0.499	0.331
3.0	1.717	0.692	0.391	0.259
4.0	1.452	0.508	0.269	0.179
5.0	1.327	0.403	0.206	0.138
$R \rightarrow \infty$	1.250	$2/R$	$1/R$	$2/3R$

$R$ [ $a_0$ ]	$J_1$ [mRy]	$V_1$ [mRy]	$V_2$ [mRy]
2.0	9.54	-18.07	33.58
2.5	7.39	-17.45	19.58
3.0	5.59	-16.08	11.95
4.0	2.90	-12.92	4.49
5.0	1.26	-9.64	1.56
$R \rightarrow \infty$	$\frac{4R^3}{15} e^{-R} \log R$	$2R e^{-R}$	$4R e^{-2R}$

The inclusion of the full Coulomb potential (4) will introduce three-site terms already in the hopping integral  $t'_{ij}$  in the atomic basis; this feature follows the definitions and expressions for *all* the interaction parameters for the Wannier function (2) provided in Appendix A (Ref.<sup>8</sup> does not contain all parameters explicitly and the evaluation of  $t_{ij}$  is absent, see Appendix B). Also, the outlines of the diagonalization method and of the single-particle-basis optimization are briefly summarized in Appendix C. In what follows we concentrate on the physical properties of the results for a linear chain with periodic boundary conditions containing up to  $N = 12$  atoms. Particular emphasis is put on the asymptotic properties (i.e. those weakly dependent on  $N$ ) of those truly nanoscopic systems depicted schematically in Fig. 1.

### III. METALLIC AND MOTT LOCALIZED STATES

#### A. Band energy and the effective band mass

We begin with the whole analysis of the band electron properties. The values of atomic level position  $\epsilon_a = \int d^3\mathbf{r} w_i^*(\mathbf{r}) T(\mathbf{r}) w_i(\mathbf{r})$  and of the hopping matrix elements  $t_m = \int d^3\mathbf{r} w_i^*(\mathbf{r}) T(\mathbf{r}) w_{i+m}(\mathbf{r})$  with  $m = 1, \dots, 5$  are listed in Table II for  $R/a_0 = 2 \div 5$ . At most, three first hopping matrix elements are important; this is sufficient to achieve the asymptotic properties already for  $N \geq 8$ . Such a fast diminution of  $t_m$  with increasing  $m$  is due to the reduction of the spread of the Wannier functions  $\{w_i(\mathbf{r})\}$  due to the intersite repulsive Coulomb interaction<sup>9</sup>. The space profile of the Wannier function along the chain direction for different interatomic distances is shown in Fig. 2. The wave-function renormalization is apparent for smaller  $R/a_0$ , where metallic state is expected to appear.

From Table II one can also see that the atomic energy is strongly dependent on the distance  $R$  and even for  $R = 5a_0$  it is decisively lower ( $\approx -2.7$  Ry) than that in the 1s state of hydrogen atom ( $-1$  Ry). This decrease is caused both by the long-range nature of the attractive potential  $V(\mathbf{r})$ .

The band energy can be calculated directly by introducing the corresponding single-particle energy

$$\epsilon_n = \sum_{m=0}^{N-1} t_m \cos\left(\frac{2\pi m k_n}{N}\right), \quad (5)$$

where  $k_n = -[N/2], \dots, [(N-1)/2]$  ( $[x]$  denotes the integer part of  $x$ ) is the quantum number (related to the wavevector via relation  $k = 2\pi k_n/NR$ ) in the first Brillouin zone. The profile of the bands evolving with the increasing lattice parameter  $R$  is shown in Fig. 3ab. Only for the distances  $R \gtrsim 4a_0$  we can approximate the band with one hopping parameter  $t_1$ , when the bandwidth is strongly reduced, as one would expect on the basis of the tight-binding-approximation (TBA). The Fermi level is always at the point  $kR/\pi = 0.5$ , as we have assumed that we have one electron per atom.

From the band energies we can obtain the effective band mass at either the band center ( $k = 0$ ) or at the Fermi point ( $k_F = \pi/2R$ ):

$$m_0^* = \hbar^2 \left( \frac{d^2\epsilon_k}{dk^2} \Big|_{k=0} \right)^{-1} \stackrel{\text{a.u.}}{=} \frac{2}{R^2} \left( \frac{d^2\epsilon_k}{dk^2} \Big|_{k=0} \right)^{-1}, \quad (6)$$

$$m_F^* = \hbar^2 k_F \left( \frac{d\epsilon_k}{dk} \Big|_{k=k_F} \right)^{-1} \stackrel{\text{a.u.}}{=} \frac{\pi}{R^2} \left( \frac{d\epsilon_k}{dk} \Big|_{k=\pi/2} \right)^{-1}. \quad (7)$$

The relative effective mass  $m^*/m_e$  (where  $m_e$  is the free rest mass) are plotted in Fig. 4ab (the inaccuracies are due to the numerical differentiation of  $\epsilon_k$ ). The mass grows with the increasing interatomic distance and reaches about 50–70% higher value (then  $m_e$ ) for  $R/a_0 \approx 5$ . One should also note that even though the Wannier functions are obtained from optimizing the energy of the interacting state, the masses are light ( $m^* < m_e$ ) for  $R \leq 3.5a_0$ . What is more important, they practically do not depend on  $N$  for  $N \geq 6$ . Therefore, in Fig. 5 we have plotted the profile of  $m^*/m_e$  only for  $N = 10$  versus both  $R/a_0$  and  $kR/\pi$ .

The calculated band energies will serve as an input in the discussion of the relative role of the Coulomb interaction at the onset of the Mott localized state. This is considered next by determining first the bare bandwidth  $W = 2 \left| \sum_{m=1}^{N-1} t_m \right|$  and comparing it with the magnitude of the effective Coulomb interaction.

#### B. Onset of the Mott localized state

The determination of the basis  $\{w_i(\mathbf{r})\}_{i=1, \dots, N}$  allowed for determination of the interaction parameters (cf. Table I) and the hopping integrals  $t_m$  (cf. Table II). Therefore, the bare bandwidth can be also defined as

$$W = \max\{\epsilon_k\} - \min\{\epsilon_k\}. \quad (8)$$

In Table III we present (for  $N = 8$ ) the effective orbital size  $a_H = \alpha_{\min}^{-1}$  (in units of  $a_0$ ), the bandwidth  $W$ , the effective interaction parameters  $U - K_1$ , the  $W/(U - K_1)$  ratio, and the product of the carrier density  $n_C = 1/R$  and the optimal orbital radius  $a_H = \alpha_{\min}^{-1}$ . The product  $n_C a_H$  illustrates the Mott criterion for localization<sup>10</sup>, which can be generalized first to the case of  $d$ -dimensional infinite lattice, which takes the form  $n_C^{1/d} a_H \approx 0.2$ . The critical value of the product 0.2 is reached for  $R \approx 4.5a_0$  and hence we should ask, whether this is a coincidence or if it reflects the localization onset for the correlated electrons in these nanoscopic systems. This criterion is not strongly dependent on  $N$ , as shown in Fig. 6 and hence represents an intrinsic property, independent of the system size for  $N \geq 8$ .

TABLE II. Single-particle parameters versus interatomic distance for  $N = 10$  sites.

$R/a_0$	$\epsilon_a$ [Ry]	$t_1$ [Ry]	$t_2$ [mRy]	$t_3$ [mRy]	$t_4$ [mRy]	$t_5$ [mRy]
2.0	-4.461	-0.585	87.0	-8.93	1.29	-0.413
2.5	-4.077	-0.330	44.0	-4.10	0.54	-0.154
3.0	-3.712	-0.200	23.6	-2.00	0.23	-0.006
3.5	-3.399	-0.127	13.0	-0.99	0.10	-0.002
4.0	-3.138	-0.083	7.5	-0.54	0.05	-0.009
4.5	-2.920	-0.055	8.2	-0.66	0.05	-0.008
5.0	-2.737	-0.037	4.3	-0.28	0.02	-0.002

For that purpose we have calculated basic quantities signalling such a crossover, each of which can be characterized briefly under the following headings:

- (i) The total *spin length* per site. We characterize it by its square, i.e. by  $\langle \mathbf{S}_i^2 \rangle = \langle 0 | \mathbf{S}_i^2 | 0 \rangle$ , where  $\mathbf{S}_i = (S_i^+, S_i^-, S_i^z) = (a_{i\uparrow}^\dagger a_{i\downarrow}, a_{i\downarrow}^\dagger a_{i\uparrow}, (n_{i\uparrow} - n_{i\downarrow})/2)$  is the electron spin operator for the atomic site  $i$ . It is easy to prove<sup>11</sup> that

$$\langle \mathbf{S}_i^2 \rangle = \frac{3}{4} (1 - 2 \langle n_{i\uparrow} n_{i\downarrow} \rangle). \quad (9)$$

Therefore, in the atomic limit with one electron per atom we have that  $d^2 \equiv \langle n_{i\downarrow} n_{i\uparrow} \rangle = 0$  and hence the spin length acquires the Pauli-spin limit  $S(S+1) = 3/4$ . In the opposite, Hartree-Fock limit ( $U_{\text{eff}} \ll W$ ),  $\langle n_{i\uparrow} n_{i\downarrow} \rangle = 1/4$ , and  $\langle \mathbf{S}_i^2 \rangle = 3/8$ . Hence, the quantity  $\Theta_M = (4/3) \langle \mathbf{S}_i^2 \rangle$  starts from the value 1/2 for  $R \rightarrow 0$  and approaches the value of unity when the atomic-like localized states are more proper. Note that the ground state of the system is always a total spin singlet, i.e.  $\langle 0 | \sum_{i=1}^N \mathbf{S}_i | 0 \rangle = 0$ .

- (ii) The dispersion of the statistical distribution of function  $n_{k\sigma} = \langle 0 | a_{i\sigma}^\dagger a_{i\sigma} | 0 \rangle \equiv \langle 0 | \hat{n}_{k\sigma} | 0 \rangle$ . The distributions in both the optimized correlated state (i.e. with  $\alpha = \alpha_{\min}$ ) and in the state without such an optimization (i.e. for  $\alpha = a_0^{-1}$ ) is displayed in Fig. 7ab. As the case with the optimized size  $\alpha^{-1} = \alpha_{\min}^{-1}$  has a lower energy (see below), the behavior of  $n_{k\sigma}$  confirms the existence of the Fermi ridge at  $k = k_F = \pi/2R$  for  $R \sim 2a_0$  followed by its gradual diminution to its disappearance with the increasing  $R$ . The presence of the Fermi ridge speaks directly in favour of delocalized (metallic) state of electrons<sup>12</sup>. The distribution for  $R \lesssim 4a_0$  is essentially the Fermi-Dirac distribution modified by the Fermi liquid effects, which is smeared out completely for  $R > 5a_0$ . To put this process on the quantitative grounds we have calculated first the dispersion of the statistical distribution

$$\begin{aligned} \sigma^2\{n_{k\sigma}\} &= \frac{1}{2N} \sum_{k\sigma} \langle 0 | \hat{n}_{k\sigma} | 0 \rangle^2 \\ &- \left( \frac{1}{2N} \sum_{k\sigma} \langle 0 | \hat{n}_{k\sigma} | 0 \rangle \right)^2. \end{aligned} \quad (10)$$

In the Hartree-Fock limit this quantity can be calculated by assuming that  $\langle \hat{n}_{k\sigma} \rangle = \Theta(\mu - \epsilon_k)$ , so that  $\sigma^2\{n_{k\sigma}\} = 1/4$ , whereas it vanishes for the even momentum distribution ( $n_{k\sigma} = 1/2$ ), when the particle position is sharply defined on atom, i.e. for the localized states reducing to the atomic states.

- (iii) The nearest neighbor *spin-spin correlation function*  $\Theta_{\text{AF}} = -\langle \mathbf{S}_i \cdot \mathbf{S}_{i+1} \rangle$ . It should be zero in the Hartree-Fock limit and reach the value (3/4) for the nearest-neighbor singlet state which mimics the antiparallel orientation of the classical spins.

- (iv) The *Fermi discontinuity* (ridge) *disappearance*. It is defined as<sup>12</sup>

$$\Delta n_{k_F} = n_{k=k_F-0} - n_{k=k_F+0}. \quad (11)$$

This difference has been interpolated by a parabola  $n_{k\sigma} = \alpha k^2 + \beta k + \gamma$  from both sides leading to the value  $\Delta n_{k_F}^{\text{par}}$  at the jump. Such an interpolation simulates a quasicontinuous function  $n_{k\sigma}$ , which would be present for large  $N$ . The resultant  $R$  dependences of both computed and interpolated  $\Delta n_{k_F}$  values for  $N = 10$  are listed in Table IV. The discontinuity disappears in the range of  $R_c = 4 \div 4.5a_0$ . The large uncertainty is due to the poor statistics of the points (3 points on each side). However, it is close to the values deducted from  $R$  dependence of the quantities (i)-(iii), as we discussed next.

The quantities characterized (i)-(iii) are displayed in Fig 8, where we have shadowed the difference between the results for  $N = 6$  and 10 (the results for  $N = 8$  fall in the area) to amplify the convergence of the numerical results. We see that the quantities  $\Theta_M$ ,  $\Theta_{\text{AF}}$ , and  $\Theta_M$  acquire the atomic values within the 5% range for  $R/a_0 \approx 5$ , which corresponds to the interatomic distance  $R \approx 2.6 \text{ \AA}$ . It should be underlined that we do not expect any discontinuous phase transition for this finite (in fact, nanoscopic!) system. However, with the help of the characteristics provided above one can define an experimental criterion of localization (here we suggest that the 5% margin for the characteristics to fall within the atomic limit values, is a natural one). Also, all the characteristics defined above are defined from the side of the delocalized (metallic) state. To define properly the Mott insulating state as that of a Heisenberg magnet (i.e. with frozen orbital degrees of freedom), we have to consider the spin-spin correlation function directly, as well as the magnitude of the superexchange (kinetic exchange), both as a function of interatomic distance.

TABLE III. Effective Bohr radius ( $a_H$ ), the bare bandwidth ( $W$ ), the interaction parameter ( $U - K_1$ ), the bandwidth to interaction ratio, and the Mott criterion ( $n_{caH}$ ), respectively.

$R/a_0$	$a_H/a_0$	$W$	$U - K_1$	$W/(U - K_1)$	$n_{caH}$
2.0	0.570	2.381	1.224	1.945	0.285
2.5	0.667	1.340	1.106	1.212	0.267
3.0	0.750	0.810	1.026	0.790	0.250
3.5	0.818	0.512	0.976	0.525	0.234
4.0	0.874	0.333	0.944	0.353	0.219
5.0	0.948	0.148	0.925	0.160	0.190

The Fermi ridge is sharply defined in the many-fermion system only when the perturbation expansion is convergent (cf. Luttinger<sup>12</sup>). It is certainly not at the Mott metal-insulator transition. Our results show that the Fermi discontinuity disappears with the increasing lattice parameter even in the situation when we have a crossover transition from a metal to an insulator. This means that low-dimensional (finite) systems cannot always be analyzed perturbationally even though they do not exhibit phase transformation in the thermodynamic sense. Obviously, part of the jump at the Fermi points is due to the discreteness of the particle quasimomentum in this finite-size system.

#### IV. KINETIC EXCHANGE AND SPIN-SPIN CORRELATIONS

In our system the total spin is conserved. Since the ground state is a spin singlet, we have that  $\langle 0 | \left( \sum_{i=1}^N \mathbf{S}_i \right)^2 | 0 \rangle = 0$ . From this we can derive the sum rule for the ground state of the Heisenberg system in the form

$$\langle \mathbf{S}_i^2 \rangle + \sum_{m=1}^{N-1} \langle \mathbf{S}_i \cdot \mathbf{S}_{i+m} \rangle = \frac{1}{N} S_{\text{tot}} (S_{\text{tot}} + 1) = 0. \quad (12)$$

In our case the spins are defined in the Fock space (see above). Therefore, the sum rule may not be obeyed, since the spin magnitude is smaller. This is explicitly evident in Table V, where the spin-spin correlation functions  $\langle \mathbf{S}_i \cdot \mathbf{S}_{i+m} \rangle$  are listed as a function of  $R$ . The long-range correlations set in and oscillate in sign as the atomic limit is approached. This feature of the correlation function must be induced by the Anderson antiferromagnetic kinetic exchange interaction. We have calculated the kinetic exchange integrals between  $m$ -th neighbors defined as<sup>13</sup>

$$J_{\text{kex}}^{(m)} = \frac{4(t_m + V_m)^2}{U - K_m}, \quad (13)$$

and displayed them in Table VI. The total strength of kinetic exchange ( $\approx \sum_{m=1}^3 J_{\text{kex}}^{(m)}$ ) has also been compared with the corresponding quantity ( $\approx \sum_{m=1}^3 J_m$ ) expressing the strength of the Heisenberg-Dirac exchange (the former dominates in the full  $R$  range listed). Obviously, Eq. (13) provides, strictly speaking, the reliable values for the kinetic exchange integral only in the limit  $U - K_m \gg |t_m + V_m|$ . All the integrals are of antiferromagnetic character, since they express virtual hopping processes between  $m$ -neighbors, which occur (and diminish the system energy in the second order) only when spins on the two sites are oriented antiparallel. The results for the integrals  $J_{\text{kex}}^{(m)}$  are only weakly dependent on  $N$ , as exemplified in Fig. 9ab, where the first two exchange integrals have been shown for  $N = 6, 8, 10$ . The

kinetic exchange is rather strong as for e.g.  $R = 2.65 \text{\AA}$  we have that  $J_{\text{kex}}^{(1)} = 0.124 \text{ eV}$  ( $\approx 1440 \text{ K}$ ),  $J_{\text{kex}}^{(2)} = 1.6 \text{ meV}$  ( $\approx 19 \text{ K}$ ),  $J_{\text{kex}}^{(3)} = 0.44 \text{ meV}$  ( $\approx 5 \text{ K}$ ). Such a strong superexchange is observed only in the two-dimensional superconducting cuprates<sup>14</sup>.

The strong system-size dependence of the spin-spin correlation functions is shown in Fig. 10a-c. This is not strange, since the spins correlate over much longer distance than the range of the interactions as express collective properties of the system (the same can be said about the Fermi discontinuity  $\Delta n_{k_F}$ ).

TABLE IV. The  $R$  dependence of the Fermi discontinuity  $\Delta n_{k_F=\pi/2R}$  and the value obtained by the parabolic interpolation  $\Delta n_{k_F}^{\text{par}}$ .

$R/a_0$	$\Delta n_{k_F}$	$\Delta n_{k_F}^{\text{par}}$
2.0	0.8264	0.7326
2.5	0.6148	0.4244
3.0	0.4033	0.1582
3.5	0.2645	0.0358
4.0	0.1791	-0.0040
4.5	0.1232	-0.0140
5.0	0.0857	-0.0130

TABLE V. The spin-spin correlation functions  $\langle \mathbf{S}_i \cdot \mathbf{S}_{i+p} \rangle$  for  $p = 1, 2, 3$  and  $N = 10$ , as a function of lattice constant.

$R/a_0$	$\langle \mathbf{S}_i \cdot \mathbf{S}_{i+1} \rangle$	$\langle \mathbf{S}_i \cdot \mathbf{S}_{i+2} \rangle$	$\langle \mathbf{S}_i \cdot \mathbf{S}_{i+3} \rangle$
2.0	-0.2959	0.0431	-0.0951
2.5	-0.3748	0.0845	-0.1399
3.0	-0.4467	0.1230	-0.1793
3.5	-0.4968	0.1501	-0.2052
4.0	-0.5277	0.1668	-0.2200
4.5	-0.5442	0.1754	-0.2241
5.0	-0.5477	0.1762	-0.2175

TABLE VI. Distance dependence of kinetic exchange integrals  $J_{\text{kex}}^{(m)}$  for  $m = 1, 2, 3$ , as well as the total kinetic exchange and the summary direct exchange integral ( $\sum J_m$ ).

$R/a_0$	$J_{\text{kex}}^{(1)}$ [Ry]	$J_{\text{kex}}^{(2)}$ [mRy]	$J_{\text{kex}}^{(3)}$ [mRy]	$\sum J_{\text{kex}}^{(m)}$ [Ry]	$\sum J_m$ [mRy]
2.0	1.190	37.34	0.493	1.227	11.98
2.5	0.438	11.67	0.129	0.450	8.37
3.0	0.183	3.99	0.036	0.187	5.99
3.5	0.082	1.39	0.010	0.084	4.25
4.0	0.039	0.48	$2.7 \cdot 10^{-3}$	0.039	2.96
4.5	0.019	0.42	$2.5 \cdot 10^{-3}$	0.019	1.99
5.0	$9.3 \cdot 10^{-3}$	0.12	$4.4 \cdot 10^{-4}$	$9.4 \cdot 10^{-3}$	1.27

## V. ELECTRON-LATTICE INTERACTION, ZERO-POINT MOTION AND DIMERIZATION FROM THE FIRST PRINCIPLES

### A. General form of local electron-phonon coupling

We can extend our method to include the local electron-lattice coupling<sup>15</sup>. In the second-quantized Hamiltonian of general form (1) the positions of nuclei  $\{\mathbf{R}_i\}_{i=1,\dots,N}$  are regarded as fixed, i.e. the ions are regarded as classical objects. If their positions are subject to a local shifts  $\{\delta\mathbf{R}_i\}_{i=1,\dots,N}$ , then the Hamiltonian will change by the amount  $\delta\mathcal{H}$ , so that now  $\mathcal{H} \rightarrow \mathcal{H} + \delta\mathcal{H}$ . The amount of the change can be calculated as

$$\delta\mathcal{H} \equiv \sum_{i=1}^N \frac{\delta\mathcal{H}}{\delta\mathbf{R}_i} \cdot \delta\mathbf{R}_i \equiv \sum_{i=1}^N \nabla_i \mathcal{H} \cdot \delta\mathbf{R}_i, \quad (14)$$

which holds true for  $|\delta\mathbf{R}| \ll R$ . Primarily, the nuclei shifts  $\{\delta\mathbf{R}_i\}$  is felt by the potential energy  $V(\mathbf{r}) \equiv \sum_i V(\mathbf{r} - \mathbf{R}_i)$  and by the Wannier functions  $\{w_i(\mathbf{r}) = w_i(\mathbf{r} - \mathbf{R}_i)\}$ . These changes, in turn, induce the alteration of the microscopic parameters  $\epsilon_a$ ,  $U$ ,  $K_{ij}$ , etc. In result, we can write the Hamiltonian change in the form

$$\begin{aligned} \delta\mathcal{H} = & \sum_i \frac{\delta\epsilon_a}{\delta\mathbf{R}_i} \Big|_0 \cdot \delta\mathbf{R}_i n_i + \\ & \sum'_{ij\sigma} \frac{\delta t_{ij}}{\delta\mathbf{R}_i} \Big|_0 (\delta\mathbf{R}_i - \delta\mathbf{R}_j) a_{i\sigma}^\dagger a_{j\sigma} + \sum_i \frac{\delta U}{\delta\mathbf{R}_i} \Big|_0 \cdot \delta\mathbf{R}_i n_{i\uparrow} n_{i\downarrow} \\ & + \sum'_{ij} \frac{\delta K_{ij}}{\delta\mathbf{R}_i} \Big|_0 \cdot (\delta\mathbf{R}_i - \delta\mathbf{R}_j) n_i n_j + \dots \end{aligned} \quad (15)$$

One should note that we have not included explicitly the more distant displacements, i.e. the terms of the type

$$\sum_{ij} \frac{\delta\epsilon_a}{\delta\mathbf{R}_j} \Big|_0 \cdot \delta\mathbf{R}_j n_i, \quad \sum_{\substack{ij\sigma \\ k \neq (i,j)}} \frac{\delta t}{\delta\mathbf{R}_k} \Big|_0 \cdot \delta\mathbf{R}_k a_{i\sigma}^\dagger a_{j\sigma}, \quad \text{etc.}$$

The last terms represent a coupling to more distant ions on the atomic level position, or on the nearest-neighbor hopping, etc. They are not included as we would like to determine first the derivatives  $\delta/\delta\mathbf{R}_i(\dots)$  from our above first-principle results (the subscript “0” means they are calculated for the periodic arrangement of ions). In Fig. 11 (bottom panel) we display the corresponding derivatives, which play the role of the local electron-lattice coupling constants, as a function of the interatomic distance. The scattering of the points is caused by the numerical differentiation. For the sake of completeness, we have plotted in the top panel the microscopic parameters vs.  $R$ , for  $N = 6 \div 10$  atoms.

There are few unique features of these results, which we would like to elaborate on. First, the interaction terms  $\sim \delta U$  and  $\sim \delta K$  diminish the system energy when the system distorts. Also,  $dU/dR \sim -d\epsilon_a/dR$ , but effectively  $|dK/dR|$  overcomes  $dt/dR$ , so that the net effects in the insulating state  $\{\hat{n}_i = 1\}$  favours the system distortion (note a rather weak dependence on  $N$ ). Furthermore, the coupling constants are relatively large. For example,  $\lambda_a/|\delta R| \equiv d\epsilon_a/dR \approx 0.5 \text{ Ry}/a_0$  we obtain for the distortion  $|\delta R|/R \approx 0.1$  (estimating the of zero-point motion amplitude; see below) the value of  $\lambda_a \approx 2 \text{ eV}$  for  $R/a_0 = 3$  (i.e.  $R = 1.6 \text{ \AA}$ ). Similarly  $\lambda_U \equiv (dU/dR)|\delta R| \approx -2.4 \text{ eV}$ ,  $\lambda_K \approx -1.6 \text{ eV}$ ,  $\lambda_t \approx 0.7 \text{ eV}$ . They represent a sizeable fraction of the value  $U - K_1 \approx 13.8 \text{ eV}$ . What is more important,  $\lambda_U/W \approx 0.25$ . However, the kinetic exchange integral is  $J_{\text{ex}}^{(1)} \approx 2.5 \text{ eV}$ , a value close to  $|\lambda_U|$ . This means that for the linear chain of hydrogen atoms the electron-lattice and magnetic interactions are of comparable magnitude. In the system with heavier ions the electron-lattice coupling should be divided roughly by  $M_i^{1/2}$ , where  $M_i$  is the ion mass. Also, in the insulating state the  $U$  and  $K$  parameters (and their derivatives) should be roughly diminished by the relative dielectric constant  $\epsilon$  of the medium. Roughly,  $(M_i/M_H)^{1/2} \sim 5 \div 10$ , and also  $\epsilon \sim 5 \div 10$ , so that the proportions between the above parameters should remain of the same order even though their absolute values diminish by the factor  $5 \div 10$ . But this means that the analysis of the strongly correlated low-dimensional systems should include on equal footing both local electron-electron and electron-lattice couplings. There are quite few relevant parameters ( $\epsilon_a, W, U, K_m, \lambda_a, \lambda_K, \lambda_U$ ) in that situation, so the usual approach of solving Hamiltonian  $\mathcal{H} + \delta\mathcal{H}$  by regarding all those quantities as free parameters of the model, does not look promising. Our first-principle approach determines the value of the parameters accurately so their values are known for fixed  $R$ . However, needless to say that our method must be extended to a more realistic situation involving e.g.  $(\text{CuO}_2)_n$  planar clusters to be applicable to the high- $T_c$  systems.

The solution of the Hamiltonian incorporating the electron-lattice interactions requires a separate analysis and will not be discussed here. In the remaining part, we concentrate only on the evolution of the zero-point motion and of the dimerization as a function of interatomic distance.

### B. Zero-point motion

In the harmonic approximation the acoustic phonons for the linear chain have the dispersion relation of the form

$$\omega_k = 2 \left( \frac{C}{M} \right)^{\frac{1}{2}} \sin \left( \frac{\pi k}{N} \right), \quad (16)$$

where  $M$  is the ion mass (we take the proton mass here) and  $C$  is the elastic constant, which can be calculated for longitudinal modes from the differentiation of the total ground state energy  $E_G$  (with inclusion of the interionic interactions), namely

$$C = \frac{1}{N} \frac{\partial^2 E_G}{\partial^2 R}. \quad (17)$$

One should note that due to the global instability ( $\partial E_G / \partial R < 0$ ) we should place the system in a box stabilizing it (e.g. the system represents a linear ring on a substrate stabilizing its geometry). Also, the  $k = 0$  is a Goldstone mode, so we select the values of  $k = 1, 2, \dots, N-1$ , i.e. chose the center-of-mass reference system. In result, the contribution of zero-point motion to the system energy is

$$\Delta E_G^{\text{ph}} = \sum_k \frac{1}{2} \hbar \omega_k = \frac{\hbar}{M^{\frac{1}{2}}} \left( \frac{1}{N} \frac{\partial^2 E_G}{\partial R^2} \right)^{\frac{1}{2}} \sum_{k=1}^{N-1} \sin \left( \frac{\pi k}{N} \right). \quad (18)$$

In the atomic units, it takes the form

$$\Delta E_G^{\text{ph a.u.}} \left( \frac{2m}{M} \right)^{\frac{1}{2}} \left( \frac{1}{N} \frac{\partial^2 E_G}{\partial R^2} \right)^{\frac{1}{2}} \sum_{k=1}^{N-1} \sin \left( \frac{\pi k}{N} \right). \quad (19)$$

To estimate the amplitude  $\Delta R$  of zero-point motion we note that quasiclassically we can write for the individual normal mode that

$$\frac{1}{2} M \omega_k^2 (\Delta R_k)^2 = \frac{1}{2} \hbar \omega_k, \quad (20)$$

where  $\Delta R_k$  is the classical amplitude of the vibrations associated with  $k$ -th mode. Introducing the global classical amplitude

$$(\Delta R)^2 = \frac{1}{N} \sum_{k=1}^{N-1} \frac{\hbar}{M \omega_k} \quad (21)$$

we obtain in atomic units that

$$(\Delta R)^2 \stackrel{\text{a.u.}}{=} \frac{1}{N} \left( \frac{m}{2M} \right)^{\frac{1}{2}} \left( \frac{1}{N} \frac{\partial^2 E_G}{\partial R^2} \right)^{-\frac{1}{2}} \sum_{k=1}^{N-1} \frac{1}{\sin(\pi k/N)}. \quad (22)$$

Approximating the summation by integration we have that  $(\Delta R)^2$  is divergent and  $(\Delta R)^2 \sim \ln N$ . The above formula expresses the first-order contribution to the lattice dynamics. This contribution<sup>19</sup> appears on the top of the optimized energy  $E_G \equiv E_G(\alpha = \alpha_{\min}, R)$ .

### C. Lattice dimerization: Basis halving

It is well known that one-dimensional systems are unstable with respect to the dimerization (the Peierls distorted phase<sup>5</sup>). We incorporate the distorted phase into

our rigorous analysis of the ground state properties. For that purpose, we define two sets of atomic basis functions  $A$  and  $B$  corresponding to even and odd lattice sites, shown schematically in Fig. 12, namely

$$\Psi_i^A(\mathbf{r}) = \Psi_{2i}(\mathbf{r}), \quad \text{and} \quad \Psi_i^B(\mathbf{r}) = \Psi_{2i+1}(\mathbf{r}).$$

The index for each sublattice takes  $N_D \equiv N/2$  values (this is the *basis halving*). We construct next the two sets of the Bloch functions starting from this atomic basis, which are

$$\Phi_k^A = \frac{\mathcal{N}_k^A}{N_D^{1/2}} \sum_{j=0}^{N_D-1} \Psi_j^A \exp \left( i \frac{2\pi k j}{N_D} \right), \quad (23)$$

$$\Phi_k^B = \frac{\mathcal{N}_k^B}{N_D^{1/2}} \sum_{j=0}^{N_D-1} \Psi_j^B \exp \left( i \frac{2\pi k j}{N_D} \right), \quad (24)$$

where the quantum number  $k = 0, \dots, N_D - 1$  enumerates the points in the reduced zone ( $N_D = N/2$ ), and the normalization factors are

$$\mathcal{N}_k = \mathcal{N}_k^A = \mathcal{N}_k^B = \left[ \sum_{p=0}^{N_D-1} S_p^{AA} \cos \left( \frac{2\pi k p}{N_D} \right) \right]^{-1/2}. \quad (25)$$

The overlap integrals  $S_p$  are calculated from the prescription:  $S_{i-j}^{\alpha\beta} = S(R_{ij}^{\alpha\beta})$ , where  $\alpha, \beta = A$  or  $B$ , and  $i - j = 0, \dots, N_D - 1$ . Obviously,  $R_{ij}^{\alpha\beta} = R_{ji}^{\beta\alpha}$  and  $R_{ij}^{AA} = R_{ij}^{BB}$ ; the same symmetry is obeyed by all quantities dependent on  $R_{ij}^{\alpha\beta}$ .

Each sublattice contains only half of the total number of lattice sites. This circumstances leads to the nonorthogonality of the Bloch functions  $\langle \Phi_k^A \Phi_k^B \rangle = S_{AB}(k) \neq 0$ , even though we had before  $\langle \Phi_k \Phi_{k'} \rangle = \delta_{kk'}$ . Therefore, the orthogonalized wave functions are

$$\Phi_k^1 = \beta (\Phi_k^A + \gamma_k^* \Phi_k^B), \quad \Phi_k^2 = \beta (\Phi_k^B + \gamma_k \Phi_k^A), \quad (26)$$

with

$$\gamma_k = -\frac{S_{AB}(k)}{1 + \sqrt{1 - |S_{AB}(k)|^2}}, \quad (27)$$

and

$$\beta_k = \left[ 1 + \frac{|S_{AB}(k)|^2}{\left( 1 + \sqrt{1 - |S_{AB}(k)|^2} \right)^2} - \frac{|S_{AB}(k)|^2}{1 + \sqrt{1 - |S_{AB}(k)|^2}} \right]^{-1/2}. \quad (28)$$

The overlap integral  $S_{AB}(k)$  for the Bloch functions can be related to the overlaps  $S_p^{AB}$  between  $p$ -th neighbors located on different sublattices, namely

$$S_{AB}(k) = \mathcal{N}_k \sum_p \left[ \frac{S_p^{AB} + S_p^{BA}}{2} \cos \left( \frac{2\pi kp}{N_D} \right) + i \frac{S_p^{AB} - S_p^{BA}}{2} \sin \left( \frac{2\pi kp}{N_D} \right) \right]. \quad (29)$$

In effect, the expansion of the Wannier function in the basis of atomic functions has the form

$$w_i^\alpha = \sum_{i\beta} \beta_{i-j}^{\alpha\beta} \Psi_j^\beta, \quad (30)$$

Taking the inverse (space) Fourier transforms of the orthonormalized Bloch functions we obtain the coefficients  $\beta_{i-j}^{\alpha\beta} \equiv \beta_p^{\alpha\beta}$  in the form

$$\beta_p^{AA} = N_D^{-1} \sum_k \mathcal{N}_k \beta_k \cos \left( \frac{2\pi kp}{N_D} \right) = \beta_p^{BB}, \quad (31)$$

$$\begin{aligned} \beta_p^{AB} = N_D^{-1} \sum_k \mathcal{N}_k \beta_k & \left[ \operatorname{Re} \gamma_k \cos \left( \frac{2\pi kp}{N_D} \right) \right. \\ & \left. + \operatorname{Im} \gamma_k \sin \left( \frac{2\pi kp}{N_D} \right) \right], \end{aligned} \quad (32)$$

$$\begin{aligned} \beta_p^{BA} = N_D^{-1} \sum_k \mathcal{N}_k \beta_k & \left[ \operatorname{Re} \gamma_k \cos \left( \frac{2\pi kp}{N_D} \right) \right. \\ & \left. - \operatorname{Im} \gamma_k \sin \left( \frac{2\pi kp}{N_D} \right) \right]. \end{aligned} \quad (33)$$

Note that  $\beta_p^{AB} = \beta_{-p}^{BA}$ , in accordance with the definition of the relative distance  $R_{ij}^{\alpha\beta}$  defined in Fig. 12.

With the help of the orthonormal basis

$$\{w_i^\alpha\}_{i=0, \dots, N_D-1}^{\alpha=A, B},$$

we can define the system Hamiltonian with inclusion of *all* two-site interactions and *all* hopping properties in the following manner

$$\begin{aligned} \mathcal{H} = \sum_{i=0}^{N_D-1} \sum_{\alpha=A, B} & \{ \epsilon_\alpha n_{i\alpha} + U n_{i\alpha\uparrow} n_{i\alpha\downarrow} \\ & + \sum_{j\beta < i\alpha} \left[ \left( K_{i-j}^{\alpha\beta} - \frac{1}{2} J_{i-j}^{\alpha\beta} \right) n_{i\alpha} n_{j\beta} - 2 J_{i-j}^{\alpha\beta} \mathbf{S}_{i\alpha} \mathbf{S}_{j\beta} \right. \\ & \left. + \sum_\sigma \left( t_{i-j}^{\alpha\beta} + V_{i-j}^{\alpha\beta} (n_{i\alpha\bar{\sigma}} + n_{j\beta\bar{\sigma}}) \right) (a_{i\alpha\sigma}^\dagger a_{j\beta\sigma} + \text{h.c.}) \right] \} \end{aligned}$$

$$+ J_{i-j}^{\alpha\beta} \left( a_{i\alpha\uparrow}^\dagger a_{i\alpha\downarrow}^\dagger a_{j\beta\downarrow} a_{j\beta\uparrow} + \text{h.c.} \right) \} \}, \quad (34)$$

where the parameters are defined by the corresponding (primed) quantities in the atomic basis in the following manner

$$\epsilon_a = \sum_{q\gamma} (\beta_q^{A\gamma})^2 \epsilon'_a + 2 \sum_{\substack{q\gamma, r\delta \\ q\gamma > r\delta}} \beta_q^{A\gamma} \beta_{-r}^{A\delta} t_{q-r}^{\gamma\delta}, \quad (35)$$

$$t_p^{\alpha\beta} = \sum_{q\gamma} \beta_q^{\alpha\gamma} \beta_{p-q}^{\beta\gamma} \epsilon'_a + 2 \sum_{\substack{q\gamma, r\delta \\ q\gamma > r\delta}} \beta_q^{\alpha\gamma} \beta_{p-r}^{\beta\delta} t_{q-r}^{\gamma\delta}, \quad (36)$$

$$\begin{aligned} U = \sum_{q\gamma} (\beta_q^{A\gamma})^4 U' + 2 \sum_{\substack{q\gamma, r\delta \\ q\gamma > r\delta}} & \left[ (\beta_q^{A\gamma} \beta_r^{A\delta})^2 (K'_{q-r}^{\gamma\delta} \right. \\ & \left. + 2 J'_{q-r}^{\gamma\delta}) + 4 (\beta_q^{A\gamma})^3 \beta_r^{A\delta} V'_{q-r}^{\gamma\delta} \right], \end{aligned} \quad (37)$$

$$\begin{aligned} K_p^{\alpha\beta} = \sum_{q\gamma} (\beta_q^{\alpha\gamma} \beta_{p-q}^{\beta\gamma})^2 U' + 2 \sum_{\substack{q\gamma, r\delta \\ q\gamma > r\delta}} & \left\{ (\beta_q^{\alpha\gamma} \beta_{p-r}^{\beta\delta})^2 K'_{q-r}^{\gamma\delta} \right. \\ & \left. + 2 \beta_q^{\alpha\gamma} \beta_{p-q}^{\beta\gamma} \left[ \beta_r^{\alpha\delta} \beta_{p-r}^{\beta\delta} J'_{q-r}^{\gamma\delta} + (\beta_q^{\alpha\gamma} \beta_{p-r}^{\beta\delta} \right. \right. \\ & \left. \left. + \beta_{p-q}^{\beta\gamma} \beta_r^{\alpha\delta} \right) V'_{q-r}^{\gamma\delta} \right\}, \end{aligned} \quad (38)$$

$$\begin{aligned} V_p^{\alpha\beta} = \sum_{q\gamma} (\beta_q^{\alpha\gamma})^3 \beta_{p-q}^{\beta\gamma} U' + 2 \sum_{\substack{q\gamma, r\delta \\ q\gamma > r\delta}} & \left\{ (\beta_q^{\alpha\gamma})^2 \left[ \beta_q^{\alpha\delta} \beta_{p-r}^{\beta\delta} \right. \right. \\ & \times \left( K'_{q-r}^{\gamma\delta} + J'_{q-r}^{\gamma\delta} \right) + (\beta_q^{\alpha\gamma} \beta_{p-r}^{\beta\delta} + 3 \beta_r^{\alpha\delta} \beta_{p-q}^{\beta\gamma}) V'_{q-r}^{\gamma\delta} \\ & \left. \left. + \beta_q^{\alpha\gamma} (\beta_r^{\alpha\delta})^2 \beta_{p-q}^{\beta\gamma} J'_{q-r}^{\gamma\delta} \right\}, \right. \end{aligned} \quad (39)$$

$$\begin{aligned} J_p^{\alpha\beta} = \sum_{q\gamma} (\beta_q^{\alpha\gamma} \beta_{p-q}^{\beta\gamma})^2 U' + 2 \sum_{\substack{q\gamma, r\delta \\ q\gamma > r\delta}} & \left[ \beta_q^{\alpha\gamma} \beta_r^{\alpha\delta} \beta_{p-q}^{\beta\gamma} \beta_{p-r}^{\beta\delta} \right. \\ & \times \left( K'_{q-r}^{\gamma\delta} + J'_{q-r}^{\gamma\delta} \right) + (\beta_q^{\alpha\gamma} \beta_{p-r}^{\beta\delta})^2 J'_{q-r}^{\gamma\delta} \\ & \left. + 2 \beta_q^{\alpha\gamma} \beta_{p-q}^{\beta\gamma} \left( \beta_q^{\alpha\gamma} \beta_{p-r}^{\beta\delta} + \beta_r^{\alpha\delta} \beta_{p-q}^{\beta\gamma} \right) V'_{q-r}^{\gamma\delta} \right]. \end{aligned} \quad (40)$$

Those microscopic parameters are calculated first in the atomic basis of *s*-type functions regarding the size

$\alpha^{-1}$  of the orbitals *the same* on both sublattices. After the calculations of the electronic ground-state energy have been finished, we include, as before, the repulsion of (hydrogen) nuclei in the form (in atomic units):

$$E_{N-N} \stackrel{\text{a.u.}}{=} \sum_{\substack{i\alpha, j\beta \\ i\alpha < j\beta}} \frac{2}{R_{ij}^{\alpha\beta}}, \quad (41)$$

where each nucleus has been taken into account only once. Adding the electronic and inter-nuclear parts, we compute the ground state energy  $E_G/N$  as a function of the average interatomic distance. In Fig. 13a we show the ground-state energy for  $N = 2$  (hydrogen molecule) and for the linear rings with even number of atoms ( $N = 4, 6, 8$ ); the discussion for odd number of atoms requires a separate analysis, as the ground state configuration of nuclei is then a ionic-density wave with wave vector  $Q < \pi/R$ . This energy is minimized with respect to both  $\alpha = \alpha_{\min}$  and the interatomic distance  $R_1$  (cf. Fig. 12); in Fig. 13b we display the inverse size ( $\alpha_{\min}$ ) of the states (for  $N = 2-8$ ); they are quite close to those obtained in the undistorted case (i.e. now  $\Delta\alpha < 0.03$ ), so that the values of the microscopic parameters such as  $U$ ,  $K_1$  or  $t_1$  are not much different in both the distorted and the undistorted states. Also, our analysis, while confirming the existence of the Peierls distorted state in the finite-size systems, shows that the distortion fades away with the increasing interatomic distance.

#### D. Lattice dimerization vs. zero-point motion

The zero-point motion of ions increases the system energy and smears out their position. The dimerization diminishes the system energy and, while shifting the ionic positions relative to each other, it leaves their locations sharply defined. Both effects may be pronounced in the finite-size systems, so the question arises how those two effects compete with each other.

In Fig. 14 we compare the ground-state-energy changes due to the dimerization and to the zero-point motion for the atoms with hydrogen ionic mass. Whereas the former decreases with the increasing size (bottom panel), the latter shows the opposite trend, as was discussed in the preceding Section. For comparison, the corresponding magnitudes of the average atomic shifts are displayed in Fig. 15. Note that the dimerization persists in the localized state of atoms and disappear only for  $R/a_0 > 6$ , when the Wannier functions can be approximated with good accuracy by the atomic functions of  $1s$  type ( $\alpha^{-1} \approx a_0$ ). The zero-point vibrations of the light atoms should also contribute to the blurring of picture of the charge densities observed e.g. in the scanning tunneling microscope of these nanoscopic objects. This type of spectroscopy should be applied to the observation of those effects on a local scale.

## VI. A BRIEF OVERVIEW: NEW FEATURES

In this work we have produced a fairly complete description of one-dimensional model system by combining the *exact* diagonalization of many-fermion Hamiltonian in the Fock space with the subsequent *first-principle* readjustment of the single-particle (Wannier) function. Electron and lattice properties have been obtained as a function of the lattice parameter and the microscopic parameters have been determined explicitly. Our approach thus *extends* the current theoretical treatments<sup>2,4,19</sup> to the *strongly correlated systems* within the parametrized (second-quantized) models by providing the determination of those parameters (coupling constants) and, in turn, determining the fundamental properties of the correlated state explicitly as a function of physical parameter, the lattice spacing  $R$ . Technically, we determine at each step the microscopic parameters taking the Wannier functions with an adjusted size (starting from an exact Wannier functions for hydrogenic-like  $s$ -states), diagonalize the Hamiltonian in the Fock space with *all* pair interactions and *all* hopping integrals included, and thus obtained ground state energy is readjusted again by changing variationally the size of the orbitals, calculating the changed parameters and performing again the diagonalization in the Fock space, and so on, until the global minimum is reached for given interatomic distance (cf. Appendix C for details). This procedure is then repeated for each selected interatomic distance.

Our method of approach reveals features, which cannot be looked into when considering only the parametrized models. Firstly, the atomic part of the energy is not a constant, as it changes widely with the changing lattice constant (cf. Table II). Secondly, the crossover to the Mott localized state of electrons, as well as the lattice-dimerization evolution can be studied systematically, as the lattice expands. Thirdly, the effective masses for both band and correlated states have been determined explicitly. Fourthly, and probably most importantly, the inclusion of *all* interactions (apart from the three- and the four-site terms) was possible, as all of them are calculated explicitly (otherwise, the model would contain many parameters and become intractable or the results would be illegible).

Such a procedure has been implemented so far (on a desktop server) for one orbital-per-site model system involving linear chains and rings containing up to  $N = 12$  atoms. However, due to the strong shrinking of the Wannier functions induced by the strong correlations, the results are rapidly converging with  $N$  and for  $N \geq 8$  and provide, in our view, a realistic estimate of the local properties of those strongly correlated systems. Obviously, we must incorporate the screening by other than valence electrons, which are present in most of real systems, as well as to extend the method to  $d$ -type orbitals before the analysis will become applicable to the correlated  $3d$  systems at hand. Nonetheless, our analysis

represents to the best of our knowledge, the first attempt to marrying consistently second- and first- and second-quantization aspects of the strong electronic correlations and as such should be tested in the clearest situation. Our method leads also to a renormalized wave equation<sup>8,9</sup> for the single-particle wave function, but this feature of the method requires a separate discussion.

The method is directly applicable to the correlated quantum dots, but here we avoided introducing the trapping potential, as we would like to avoid mixing phenomenological and microscopic concepts at this stage.

In this paper we have considered only the situation with one-electron per atom corresponding to the half-filled-band situation in the metallic state. Therefore, the onset of the Mott localization washes away any Luttinger-liquid type of dynamics. Additionally, we have concentrated on static (equilibrium) properties by determining the ground-state (spin-singlet) configuration and calculating its characteristics such as statistical distribution function, spin-spin correlation function, the exchange integrals, amplitude of dimerization, etc. A direct determination of e.g. the Hubbard gap, quasiparticle properties, pairing tendencies or spin-spin charge separation requires calculation of the dynamic quantities such as the spectral-density function and the effective interaction, particularly for the systems with one or two electron holes in our starting system. The evolution of these properties as a function of interatomic distance is of fundamental importance and should be carried out next. Also, a detailed comparison of the behavior of systems with odd and even number of electrons should be made.

A separate question concerns the implementation of the wave-function optimization within the dynamical mean-field approach<sup>20</sup> in order to obtain an explicit mean-field solution of a 3d model system on the example of the 3d Hubbard model, as a function of the interatomic distance. This would also make possible a direct incorporation of the band-theoretical methods with those emphasizing the role of local electronic correlations. We should see a decisive progress in this matter soon.

Very recently, we have calculated the effective mass in the interacting system<sup>21</sup> which corresponds to the quasiparticle mass in the infinite system. It is divergent when the calculated distribution function  $n_{k\sigma}$  is interpolated into a continuous distribution with a Fermi ridge. This results complement beautifully the results of the approach presented in the present paper.

## ACKNOWLEDGMENT

The authors are grateful to their colleagues Dr. Robert Podsiadly and Dr. Włodek Wójcik and Prof. K. Rościszewski for many discussions. We are particularly grateful to Dr. Maciek Maśka from Silesian University for his insights on both analytical and numerical aspects of the project. Dr. Marcello Acquarone acquainted us with

various electron-lattice couplings. The comments made by Prof. Dieter Vollhardt from University of Ausburg and by Dr. Krzysztof Byczuk from Warsaw University are also appreciated. The work was supported by the State Committee for Scientific Research (KBN) of Poland through Grant No. 2P03B 092 18. One of us (A.R.) acknowledges the Estreicher Scholarship awarded to him by the Jagiellonian University.

## APPENDIX A: MICROSCOPIC PARAMETERS IN THE ATOMIC BASIS

In Ref.<sup>9</sup> we have expressed the parameters  $\epsilon_a$ ,  $t_{ij}$ ,  $U$ , and  $K_{ij}$  in the atomic basis using the expansion 2. Here we supplement them with the formulae for the direct exchange integral  $J_{i-j}$  and so-called correlated hopping  $V_{i-j}$ . Namely, subtracting 2 into the expressions  $J_p \equiv J_{i-j} = \langle w_i w_j | V_{12} | w_j w_i \rangle$  and  $V_p \equiv V_{i-j} = \langle w_i w_i | V_{12} | w_i w_j \rangle$  we obtain recursively

$$\begin{aligned} J_p = & \sum_q \beta_q^2 \beta_{p-q}^2 U' + 4 \sum_{\substack{qr \\ q > r}} (\beta_q \beta_{p-q}^2 \beta_r \\ & + \beta_q^2 \beta_{p-q} \beta_{p-r}) V'_{q-r} + 2 \sum_{\substack{qr \\ q > r}} \beta_q \beta_{p-q} \beta_{p-r} \beta_r (J'_{q-r} \\ & + K'_{q-r}) + 2 \sum_{\substack{qr \\ q > r}} \beta_q^2 \beta_{p-r}^2 J'_{q-r}, \end{aligned} \quad (A1)$$

$$\begin{aligned} V_p = & \sum_q \beta_q^3 \beta_{p-q} U' + 2 \sum_{\substack{qr \\ q > r}} (\beta_q^3 \beta_{p-q} + 3\beta_q^2 \beta_{p-q} \beta_r) V'_{q-r} \\ & + 2 \sum_{\substack{qr \\ q > r}} \beta_q^2 \beta_r \beta_{p-r} (2J'_{q-r} + K'_{q-r}), \end{aligned} \quad (A2)$$

where  $p, q$  and  $r = 0, 1, \dots, N-1$ , and the expansion coefficients  $\beta_p$  of the Wannier functions obey the symmetry  $\beta_p = \beta_{-p}$  (thus for  $N$  atoms there are  $N/2$  or  $(N-1)/2$  independent coefficients when  $N$  is even or odd, respectively). The primed quantities are defined in the atomic basis  $\{\Psi_j(\mathbf{r})\}_{j=1,\dots,N}$ . For example

$$\begin{aligned} J'_{ij} \equiv & \langle \Psi_i \Psi_j | V_{12} | \Psi_j \Psi_i \rangle = \int d^3 \mathbf{r} d^3 \mathbf{r}' \Psi_i^*(\mathbf{r}) \Psi_j^*(\mathbf{r}') \\ & \times V_{12}(\mathbf{r} - \mathbf{r}') \Psi_j(\mathbf{r}) \Psi_i(\mathbf{r}'). \end{aligned} \quad (A3)$$

These expressions are used when evaluating the microscopic parameters contained in the Hamiltonian. They are determined explicitly in the optimal state:  $E_G = E_{\min}(R, \alpha = \alpha_{\min})$ .

## APPENDIX B: SIGLE-PARTICLE PARAMETERS IN THE ATOMIC BASIS

The expansion (2) leads to two-site terms in the atomic energy  $\epsilon_a$  and to and three-site terms in the hopping integrals. For the sake of completeness, we start from their full expressions in the Wannier basis:

$$\epsilon_a = \sum_q \beta_q^2 \epsilon'_a + 2 \sum_{\substack{qr \\ q > r}} \beta_q \beta_r t'_{q-r}, \quad (\text{B1})$$

$$t_p = \sum_q \beta_q \beta_{p-q} \epsilon'_a + 2 \sum_{\substack{qr \\ q > r}} \beta_q \beta_{p-r} t'_{q-r}. \quad (\text{B2})$$

In these expressions the atomic energy  $\epsilon'_a$  (in atomic units) is

$$\begin{aligned} \epsilon'_a &= \left\langle \Psi_i \left| -\nabla^2 - \sum_j \frac{2}{r_j} \right| \Psi_i \right\rangle = \\ &= \alpha^2 - 2\alpha + \sum_{j \neq i} \left[ -\frac{2}{R_{ij}} + \exp(-2\alpha R_{ij}) \left( 2\alpha + \frac{2}{R_{ij}} \right) \right], \end{aligned} \quad (\text{B3})$$

where  $R_{ij} = |\mathbf{R}_i - \mathbf{R}_j|$  and  $\mathbf{r}_j = |\mathbf{r} - \mathbf{R}_j|$ . Note the appearance of the long-range part  $\sim (-2/R_{ij})$ , as one would have in the classical limit.

The evaluation of  $t'_{ij}$  is not so straightforward as one can see from the expression

$$t'_{ij} = \left\langle \Psi_i \left| -\nabla^2 - \sum_k \frac{2}{r_k} \right| \Psi_j \right\rangle = \tau_0 - 2 \sum_k \tau_{ikj}, \quad (\text{B4})$$

where  $r_k \equiv |\mathbf{r} - \mathbf{R}_k|$ ,  $\tau_0$  represent the simple part and  $\tau_{ikj}$  is the three-site part. The part  $\tau_0$  is easy to calculate, since

$$\tau_0 \equiv \langle \Psi_i | -\nabla^2 | \Psi_j \rangle = \alpha^2 e^{-\alpha R_{ij}} \left( 1 + \alpha R_{ij} - \frac{1}{3} \alpha^2 R_{ij}^2 \right). \quad (\text{B5})$$

The three-site part is more cumbersome, as it reduces to the following integral expression

$$\tau_{ikj} \equiv \int d^3r \Psi^*(\mathbf{r}_i) \frac{1}{r_k} \Psi(\mathbf{r}_j) = \frac{\alpha^3}{\pi} \int d^3r \frac{e^{-\alpha(r_i+r_j)}}{r_k}. \quad (\text{B6})$$

To calculate the integral we introduce the spheroidal coordinates  $(\lambda, \mu)$

$$\begin{aligned} a\lambda &= r_i + r_j, & a\mu &= r_i - r_j, \\ d^3r &= \frac{\pi a^3}{4} (\lambda^2 - \mu^2) d\lambda d\mu, \end{aligned} \quad (\text{B7})$$

where  $a \equiv R_{ij}$ . The regimes for  $\lambda$  and  $\mu$  are:  $1 < \lambda < \infty$ ,  $-1 < \mu < 1$ . This transformation leads to the following expression for  $r_k$

$$r_k = \sqrt{\frac{a^2}{4}(\lambda^2 - 1)(1 - \mu^2) + \left( \lambda \mu \frac{a}{2} - h \right)}, \quad (\text{B8})$$

where  $h$  is the  $z$ -coordinate of the middle point of the Coulomb potential well caused by the  $k$ -th ion (cf. Fig B16). Integrating with respect to  $\mu$  we obtain

$$\begin{aligned} \tau_{ikj} &= \frac{1}{2} \alpha^3 a^2 \int_1^\infty d\lambda e^{-\alpha a \lambda} \left\{ \left[ \lambda^2 (1 + (2h/a)^2) + b/2 \right] \times \right. \\ &\quad \times \log \frac{(2h\lambda/a - 1) - \sqrt{(2h\lambda/a - 1)^2 + b}}{(2h\lambda/a + 1) - \sqrt{(2h\lambda/a + 1)^2 + b}} + \\ &\quad + (3h\lambda/a - 1/2) \sqrt{(2h\lambda/a + 1)^2 + b} \\ &\quad \left. - (3h\lambda/a + 1/2) \sqrt{(2h\lambda/a - 1)^2 + b} \right\}, \end{aligned} \quad (\text{B9})$$

where  $b = (\lambda^2 - 1) [1 - (2h/a)^2]$ . This integral simplifies substantially if either  $k = i$  or  $k = j$ , i.e. for  $h = \pm a/2$ . Then, taking simple limiting expression we obtain that

$$\tau_{ijk} = \alpha^3 a^2 \int_1^\infty d\lambda \lambda e^{-\alpha a \lambda} = \alpha e^{-\alpha R_{ij}} (\alpha R_{ij} + 1). \quad (\text{B10})$$

Substituting (B10) to (B4) we obtain the expression for the hopping integral for  $\text{H}_2$  molecule and for the linear chain in the tight-binding approximation (cf. Ref.<sup>8</sup>).

In the general case, we have to evaluate the integral (B9) numerically. For this purpose, one makes the change of variable  $\lambda = 1/t$  to integrate over the finite interval  $0 < t < 1$  (one has to use a variable summation step, since the integrand is logarithmically divergent at  $t = 1$ ). When using the Simpson method<sup>18</sup> one has to evaluate the integrand in  $300 \div 400$  points to achieve the accuracy  $10^{-6}$  Ry; this procedure requires a neglegible time compared to that required to determine the ground state energy.

Numerical calculations of *all* hoppings  $\{t_{ij}\}_{i,j=1,\dots,N}$  can be accelerated by exploiting the problem symmetry. Among  $N(N-1)/2$  possible hoppings for the linear-chain case with periodic boundary conditions ( $t_{ij} = t_{i-j}$ ), we have only  $(N - N \bmod 2/N)$  different integrals. In case of dimerization this number is doubled, as the hopping elements change  $t_{ij} \rightarrow t_{ij}^{AA} = t_{ij}^{BB}, t_{ij}^{AB} = t_{ji}^{BA}$ . Additionally, we use the symmetry  $h \rightarrow -h$  when evaluating  $\tau_{ijk}$ .

## APPENDIX C: GROUND-STATE ENERGY EVALUATION IN THE FOCK SPACE

For  $N$  lattice sites and the grand canonical system with variable number of electrons  $N_e = 0, 1, \dots, 2N$  and the total number of electrons with the spins up  $N_\uparrow = 0, 1, \dots, N_e$ , we have the Fock (occupation-number) space  $\mathcal{H}_1 \equiv \mathcal{H}_1\{N, N_e = 0, \dots, 2N, N_\uparrow = 0, \dots, N_e\}$  of dimension  $4^N$ . Additionally, if the number of electrons is fixed at  $N_e = N$  (i.e. for the case of one electron per atom) then the Fock space  $\mathcal{H}_2 \equiv \mathcal{H}_2\{N, N_e = N, N_\uparrow = 0, \dots, N_e\}$  has reduced dimension to  $\dim \mathcal{H}_2 = \binom{2N}{N_e}$ . Moreover, if the total  $z$ -component of spin is  $S_{\text{tot}}^z = 0$  (for  $N$  even, as happens in the situation then the space  $\mathcal{H}_2\{\dots\}$ ) reduces to the space  $\mathcal{H}_3\{N, N_e = N, N_\uparrow = N/2\}$ , with the corresponding dimension  $\dim \mathcal{H}_3 = \binom{N}{N/2}^2$ . Those dimensions for  $N = 10$  are, respectively:  $\dim \mathcal{H}_1 = 1\,048\,567$ ,  $\dim \mathcal{H}_2 = 184\,756$ , and  $\dim \mathcal{H}_3 = 63\,504$ . The implementation of the translational symmetry does not influence essentially either the computing time or the memory capacity required.

The basis vectors in the Fock space are represented by the site (Wannier-state) occupancies  $\{n_{i\sigma}\}_{\substack{i=1, \dots, N \\ \sigma=\uparrow, \downarrow}}$

$$|v\rangle = |n_{1\uparrow}, \dots, n_{N\uparrow}, n_{1\downarrow}, \dots, n_{N\downarrow}\rangle. \quad (\text{C1})$$

The creation and annihilation operators are defined in a standard manner:

$$a_{i\sigma}^\dagger |..., n_{i\sigma}, \dots\rangle = (-1)^{\nu_{i\sigma}} (1 - n_{i\sigma}) |..., n_{i\sigma} + 1, \dots\rangle, \quad (\text{C2})$$

$$a_{i\sigma} |..., n_{i\sigma}, \dots\rangle = (-1)^{\nu_{i\sigma}} n_{i\sigma} |..., n_{i\sigma} - 1, \dots\rangle, \quad (\text{C3})$$

where  $\nu_{i\sigma}$  is the number of electrons in the states preceding the  $i$ -th site (including the opposite spins if  $\sigma = \downarrow$ ). We have also used the notation  $0 | \dots \rangle \equiv 0$ . The above definitions allow for an unambiguous determination of the matrix representation of the Hamiltonian. Simply, we have to determine the matrix elements  $\langle u | \mathcal{H} | v \rangle$  for  $u, v \in \mathcal{H}_3$ . In practice, the basis vectors  $\{|v\rangle\}$  are ordered as the combination series. Therefore, acting on each of them with consecutive terms of  $\mathcal{H}$ , we immediately can identify the result of the action as proper basis vector  $\{|u\rangle\}$  (or zero vector). Thus, the number of operations is equal to the number of nonzero elements  $\{\langle u | \mathcal{H} | v \rangle\}$ .

The method allows for the construction of the Hamiltonian matrix representation for which the lowest eigenvalue is the ground state energy. The physics of the problem is determined usually by  $\sim 10\%$  of the eigenvectors with the lowest eigenenergies. In this situation the Lanczos method<sup>16</sup> in the version proposed by Nishino<sup>16</sup> is most appropriate. In its latter version one uses the *cumulant expansion* containing up to  $10^2 \div 10^3$  terms for  $N = 6 \div 10$  atoms with the lattice constant  $R = 2 \div 3a_0$  (for larger  $R$  and/or smaller  $N$  the number of terms to

be included is much smaller). The numerical accuracy of the result for  $E_G$  was typically  $10^{-6}$  Ry.

The final step involved the minimization of  $E_G$  with respect to  $\alpha$  and (whenever possible) with respect to  $R$  (in the case of dimerization it is the shorter lattice constant  $R_1$ ). The minimization was carried out using respectively one- or two-dimensional *simplex method*<sup>17</sup>, with accuracy of the order  $10^{-5}$  Ry. In practice, to achieve such accuracy in the minimization process with respect to  $\alpha$  (and  $R_1$ ) one has to repeat the whole procedure  $20 \div 40$  times for the normal state and  $100 \div 200$  times for the dimerized state. The non-dimerized state has no minimum with respect to  $R$ ; this problem is elaborated on in main text (see also<sup>8,9</sup>).

One more remark. To utilize the discrete translational symmetry by shifting state  $|u\rangle$  by one lattice constant we have to introduce the basis of eigenstates of the corresponding operator  $\mathcal{R}$ , which are defined by

$$|u; k\rangle \equiv \frac{1}{N^{1/2}} \sum_{j=0}^{N-1} \exp\left(i\frac{2\pi k j}{N}\right) \mathcal{R}^j |u\rangle, \quad (\text{C4})$$

corresponding to the eigenvalues  $\exp(i2\pi k/N)$  labeled by  $k = 0, 1, \dots, N-1$ . Under such circumstances, we can consider the construction of the Hamiltonian matrix in subspaces of dimension  $\dim \mathcal{H}_3/N$  each. But then, we have to perform additional summation over  $j$ , so the number of nonzero elements will increase by factor  $\sim N$ . In effect, we do not gain much. However, in the planned by us calculations of the excited states this reduction of the Hamiltonian dimension is crucial in making the diagonalization method effective even though the number of nonzero elements remains the same. Here we do not make use of the translational symmetry.

---

<sup>1</sup> R. O. Jones and O. Gunnarson, Rev. Mod. Phys. **61**, 689 (1989); W. Pickett, *ibid.* **61**, 433 (1989); W. M. Temmerman, A. Svane, Z. Szostek and H. Winter, in *Electronic Density Functional Theory: Recent Progress and New Directions*, edited by J. F. Dobson, G. Vignale, and H. Das (Plenum, New York 1998) pp. 327-47.

<sup>2</sup> The question of importance of intersite interaction within the context of parametrized models for low-dimensional systems was addressed by a number of authors, see: J. Hubbard, Phys. Rev. B **17**, 494 (1978); J. Kondo and K. Yamai, J. Phys. Soc. Japan **43**, 424 (1977); A. A. Ovchinnikov, Mod. Phys. Lett. B, **7** 1397 (1993); S. Caponi, D. Poilblanc, and T. Giamarchi, Phys. Rev. B **61**, 13410 (2000); R. Strack and D. Vollhardt, Phys. Rev. Lett. **70**, 2637 (1993); L. Arachea and A. A. Aligia, Phys. Rev. Lett. **73**, 2240 (1994).

- <sup>3</sup> For review see: H. J. Schultz, in *Correlated Electron Systems*, edited by V. J. Emery (World Scientific, Singapore, 1993) p. 199ff; J. Voit, Rep. Prog. Phys. **57**, 977 (1995). Experimentally: C. Kim, Z.-X. Shen, N. Motoyama, H. Eisaki, S. Uchida, T. Tohyama and S. Maekawa, Phys. Rev. B **56**, 15589 (1997).
- <sup>4</sup> D. Poilblanc, S. Yunoki, S. Maekawa, and E. Dagotto, Phys. Rev. B **56**, R1645 (1997); T. Giamarchi and A. J. Millis, Phys. Rev. B **46**, 9325 (1992); S. Daul and R. M. Noack, Phys. Rev. B **61** 1646 (2000).
- <sup>5</sup> R. E. Peierls, *Quantum Theory of Solids* (Clarendon Press, Oxford, 1953) p. 108ff; M. J. Rice and S. Strässler, Solid State Commun. **13**, 125 (1973); for the discussion of relation to the charge- and spin-density wave states see e.g. S. Caprara, M. Avignon, and O. Navarro, Phys. Rev. B **61**, 15667 (2000). The quantum fluctuation in noncorrelated systems were discussed in: J. E. Hirsh and E. Fradkin, Phys. Rev. Lett. **49**, 402 (1982).
- <sup>6</sup> A. R. Goni, A. Pinczuk, J. S. Weiner, B. S. Dennis, L. N. Pfeifer, and K. West, Phys. Rev. Lett. **70**, 1151 (1993); for review see: T. Ishiguro, K. Yamaji, and G. Saito, *Organic Superconductors* (Springer Verlag, Berlin, 1998).
- <sup>7</sup> J. W. Mintmire, B. I. Dunlap, and C. T. White, Phys. Rev. Lett. **68**, 631 (1992).
- <sup>8</sup> J. Spałek, R. Podsiadły, W. Wójcik, and A. Rycerz, Phys. Rev. B **61**, 15676 (2000); for a brief review see: J. Spałek *et al.*, Acta Phys. Polonica B **31**, 2879 (2000).
- <sup>9</sup> A. Rycerz and J. Spałek, Phys. Rev. B **63**, 073101 (2001).
- <sup>10</sup> N. F. Mott, *Metal-Insulator Transitions* (Taylor and Francis, London, 1990).
- <sup>11</sup> See e.g. J. Spałek, J. Solid St. Chem. **88**, 70 (1990); J. Spałek and W. Wójcik, in *Spectroscopy of Mott Insulators and Correlated Metals*, edited by A. Fujimori and Y. Tokura (Springer Verlag, Berlin, 1995) p. 41ff.
- <sup>12</sup> The existence of the Fermi level appears also for finite  $N$  as it expresses the Pauli principle for quasiparticles (exists for example for nuclei). The existence of the Fermi discontinuity in interacting gas has been discussed by A. B. Migdal, J. Exp. Teoret. Phys. (USSR) **32**, 399 (1957) [Sov. Phys. - JETP **5**, 333 (1957)]; E. Daniel and S. Vosko, Phys. Rev. **120**, 2041 (1960); J. M. Luttinger, Phys. Rev. **119** 1153 (1960); for an interpolation between the high- and the low-density limits see e.g. N. H. March, W. H. Young, and S. Sampantar, *The Many-Body Problem in Quantum Mechanics* (Dover, New York, 1995) pp. 166-8.
- <sup>13</sup> The kinetic exchange integrals defined in this manner are well defined only in the limit  $|t_m + V_m| \ll U - K_m$ . For  $m = 1$  and neglecting  $K_m$  they were defined in P. W. Anderson, Phys. Rev. **115**, 2 (1959). In general case, they were considered in: J. Spałek, A. M. Oleś, and K. A. Chao, phys. stat. solidi (b) **108**, 329 (1981).
- <sup>14</sup> C.f. R. J. Birgenau and G. Shirane in *Physical Properties of High-Temperature Superconductors*, edited by D. M. Ginsberg (World Scientific, Singapore, 1989) vol. 1, p. 151ff and references therein.
- <sup>15</sup> The discussion here systematizes to some extent various types of local electron-lattice couplings considered earlier: A. A. Ovchinnikov, Fiz. Tverd. Tela **1**, 832 (1965) [Sov. Phys. - Solid State **7**, 664 (1965)]; T. Holstein, Ann. of Phys. **8**, 325 (1959); S. Barišić, Phys. Rev. B **22**, 2099 (1980); M. Acquarone and C. Noce, Int. J. Mod. Phys. B **13**, 3331 (1999).
- <sup>16</sup> T. Nishino and J. Kanamori, J. Phys. Soc. Japan **59**, 253 (1990); T. Nishino, *Electron Correlation Effects in Low Dimensional Periodic Systems*, unpublished. It is based on the Lanczos method: C. Lanczos, J. Res. Nat. Bur. Std. **45**, 255 (1950); see also: J. K. Cullum and R. A. Willoughby, *Lanczos Algorithms for Large Symmetric Eigenvalue Computation* (Birkhauser, Boston, 1985); E. Dagotto and A. Moreo, Phys. Rev. D **31**, 865 (1985).
- <sup>17</sup> S. Brandt, *Statistical and Computational Methods in Data Analysis* (Springer Verlag, New York, 1997).
- <sup>18</sup> See, e.g. R. L. Burden, J. D. Faires, *Numerical Analysis* (Prindle, Weber & Schmidt, Boston, 1985).
- <sup>19</sup> Earlier efforts contain an approximate treatment of correlations in 3d systems combined with the ab initio calculations of single-particle states; see: V. I. Anisimov, J. Zaanen, and O. K. Andersen, Phys. Rev. B **44**, 943 (1991) - the so-called LDA+U; J. Spałek and W. Wójcik, Phys. Rev. B **45**, 3799 (1992) - Gutzwiller approach to correlations; G. Stollhoff, Europhys. Lett. **30**, 99 (1995) - the so-called local-ansatz+LDA.
- <sup>20</sup> W. Metzner and D. Vollhardt, Phys. Rev. Lett. **62**, 324 (1989); M. Jarrell, *ibid.* **68**, 168 (1992).
- <sup>21</sup> J. Spałek and A. Rycerz, submitted to Phys. Rev. Lett.

## FIGURES

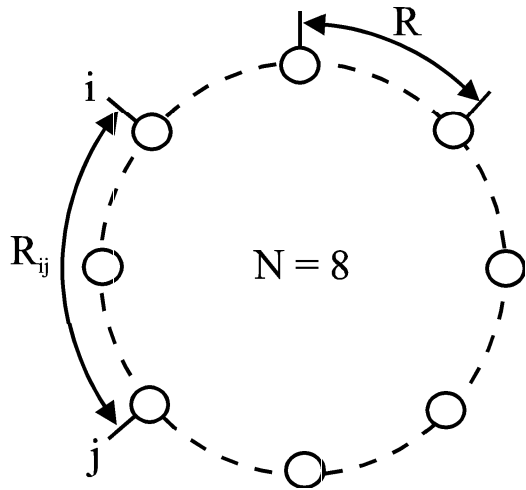


FIG. 1. Schematic representation of the finite linear chain with periodic boundary conditions used in the calculations.

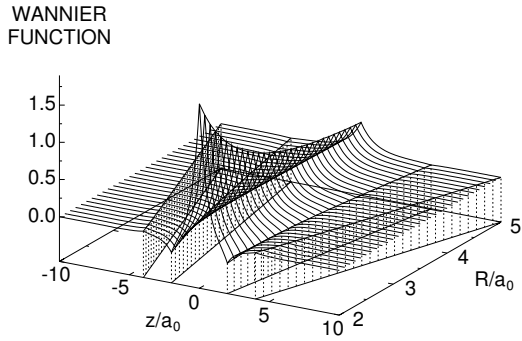


FIG. 2. Space profile of the Wannier-function evolution with the increasing interatomic distance.

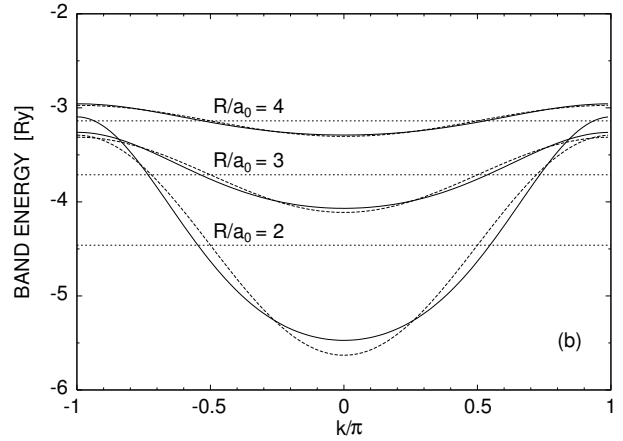
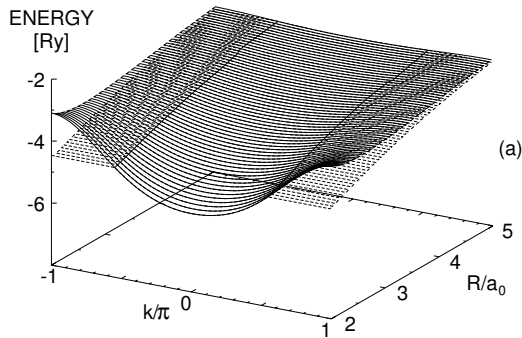


FIG. 3. a) The space profile of the band shape for  $N = 10$  versus  $R$ , taking into account the calculated hopping integrals  $\{t_m\}_{m=1,\dots,5}$ . The horizontal plane intersecting the band marks the Fermi level position; b) the flattening of the band shape with the increasing  $R$  (the dashed lines describe the band shape if only  $t_1$  is included).

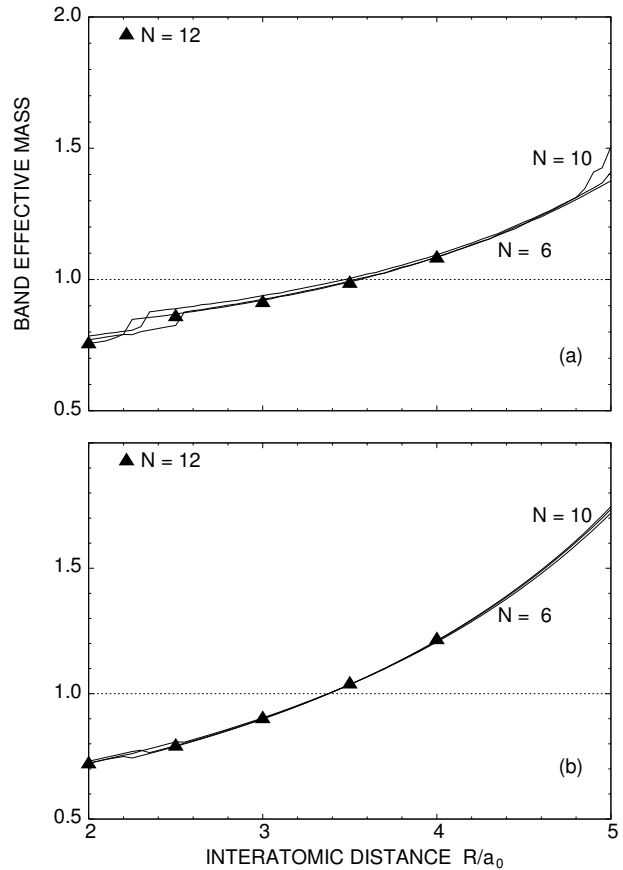


FIG. 4. a) The band effective mass at the band center ( $k = 0$ ) and b) for the Fermi wave vector  $k = k_F$ , both vs.  $R$ . Note a general insensitivity of the results for different  $N$ .

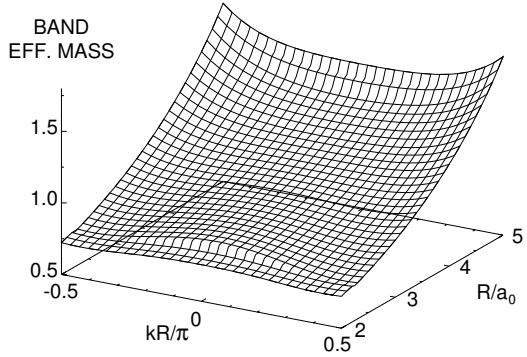


FIG. 5. The profile of the (bare) band effective mass as a function of the wave vector  $k$  and the interatomic distance  $R$  (for  $N = 10$ ).

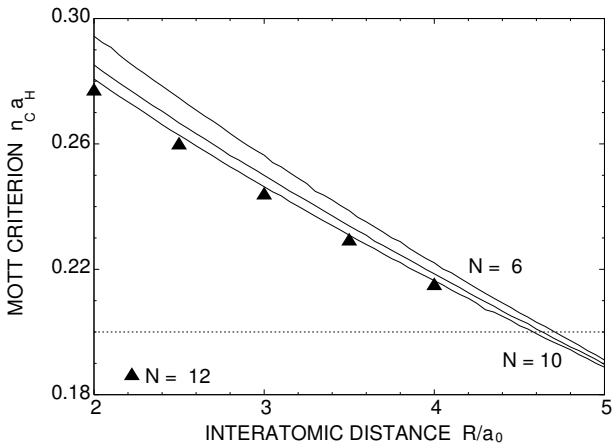


FIG. 6. The Mott-criterion value  $n_{CAH}$  vs.  $R$  and for different number of sites  $N = 6 \div 10$ . The horizontal line marks the value for bulk systems.

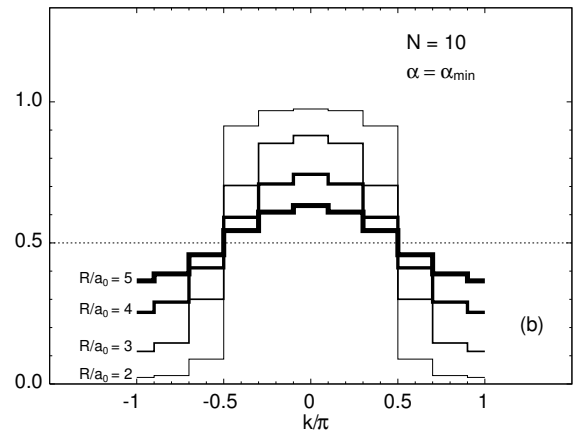
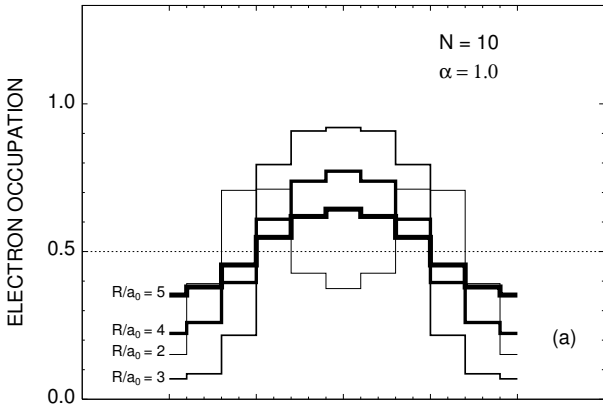


FIG. 7. The statistical distribution function  $n_{k\sigma}$  for  $N = 10$  in the state with optimized orbitals (a) and with non-optimized orbitals (b); both for different interatomic distances  $R$ .

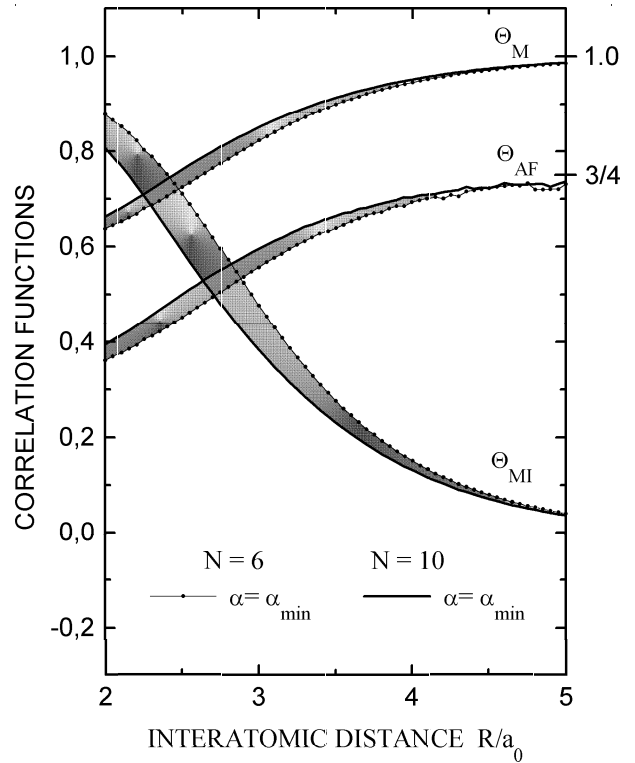


FIG. 8. Correlation functions versus distance  $R$ , characterizing the crossover from itinerant to localized state. The shaded areas are drawn to illuminate the results convergence with the increasing  $R$ .

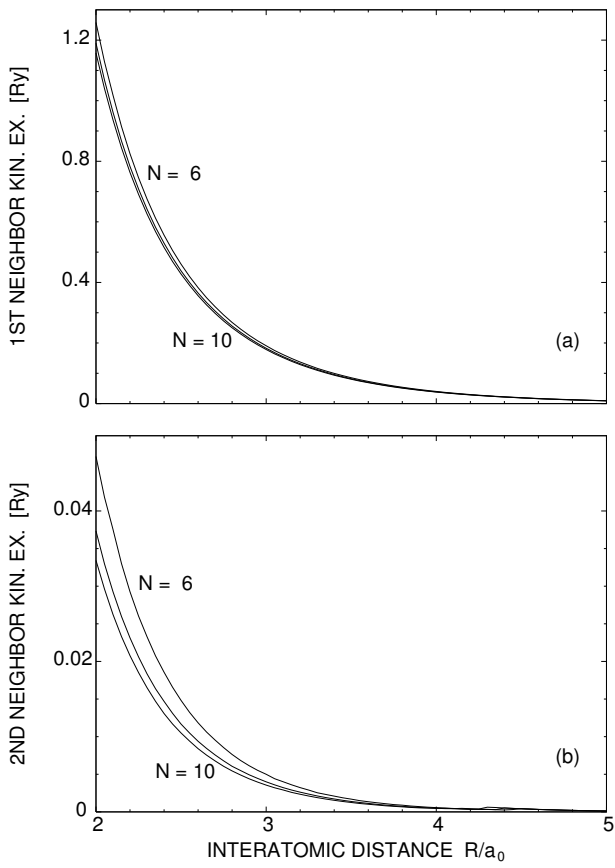


FIG. 9.  $R$  dependence of the kinetic exchange integrals  $J_{\text{kex}}^{(1)}$  (a) and  $J_{\text{kex}}^{(2)}$  (b) for different  $N = 6 \div 10$ . The results for the dominant integral (a) are weakly  $N$  dependent.

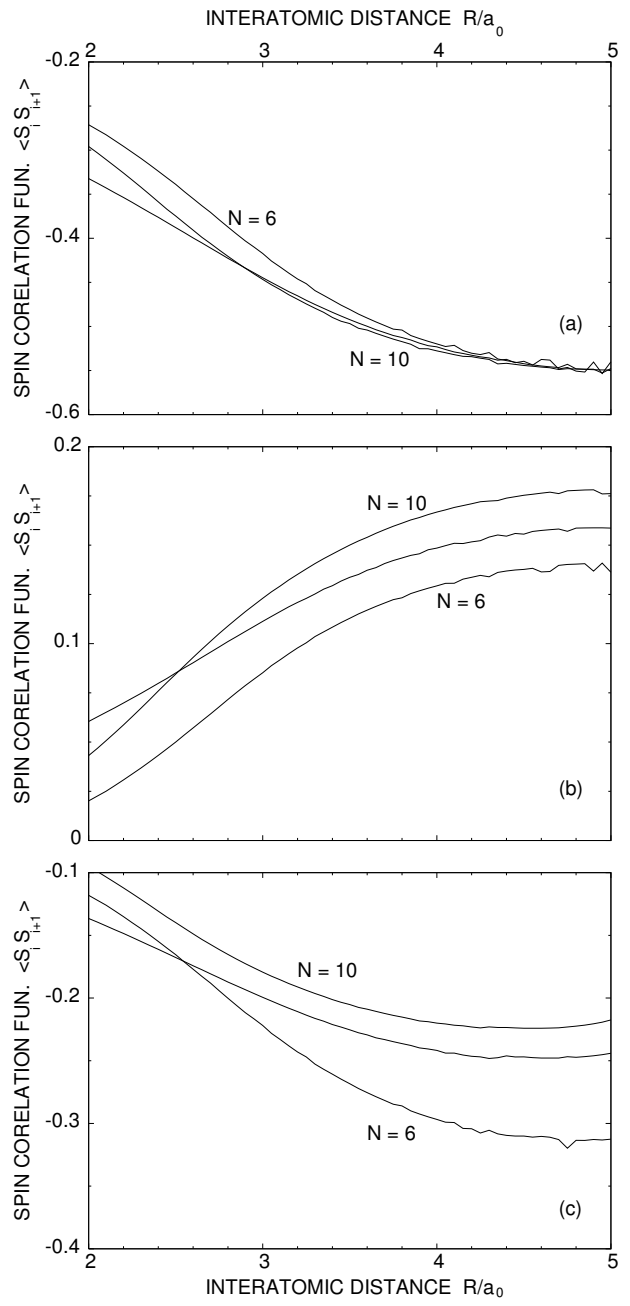


FIG. 10. Distance dependence of the spin-spin correlation functions  $\langle \mathbf{S}_i \cdot \mathbf{S}_{i+p} \rangle$  for  $p = 1 \div 3$  and  $N = 6 \div 10$ . Note the oscillatory character with  $p$  expressing the antiferromagnetic correlations.

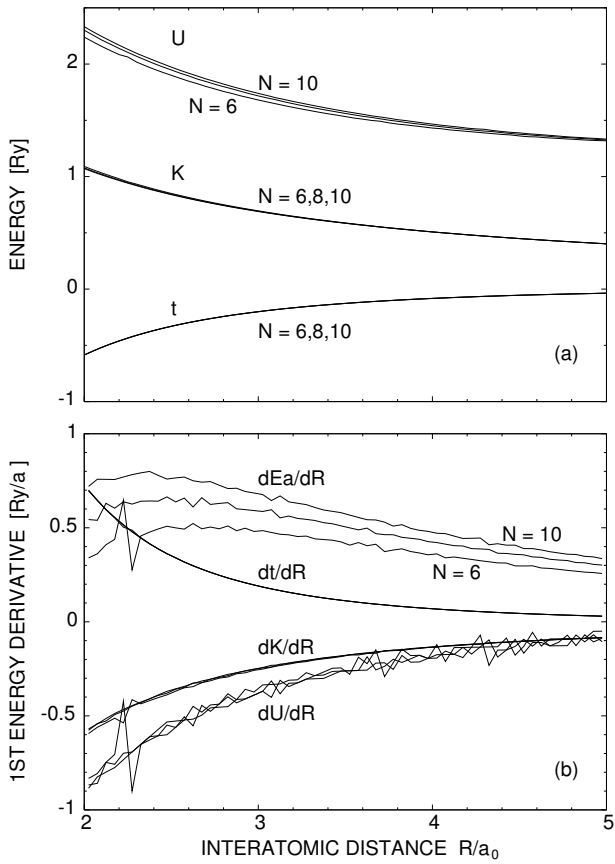


FIG. 11. The interaction parameters (a) and their derivatives (b) with respect to the lattice-parameter change; the latter express the coupling-constant strength for different local electron-lattice couplings.

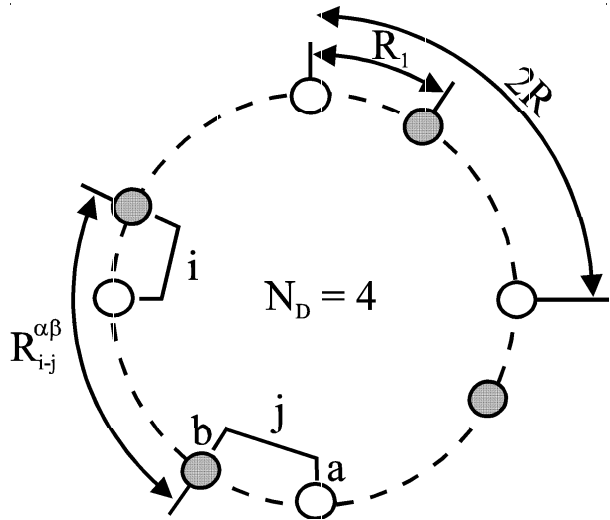


FIG. 12. Schematic representation of the chain dimerization with the characteristic distance and the distortion into two sublattices.

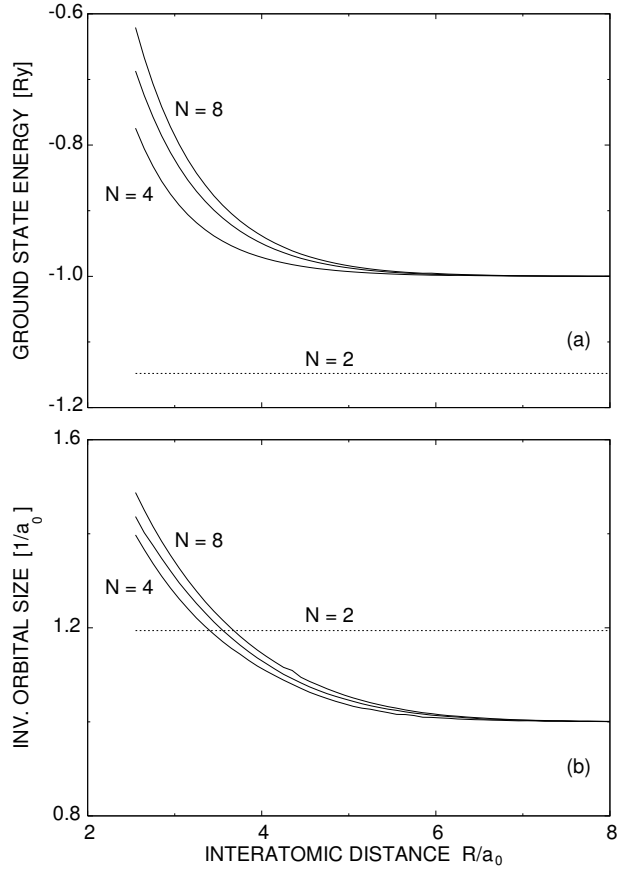


FIG. 13. Ground state energy (a) and the optimal inverse orbital size (b) of the dimerized chain versus  $R$ , for  $N = 2 \div 8$  and for the optimized both the distortion  $(1 - R_1/R)$  and the orbital size  $\alpha^{-1}$ . The dotted base lines mark the corresponding quantities for the  $H_2$ -molecule.

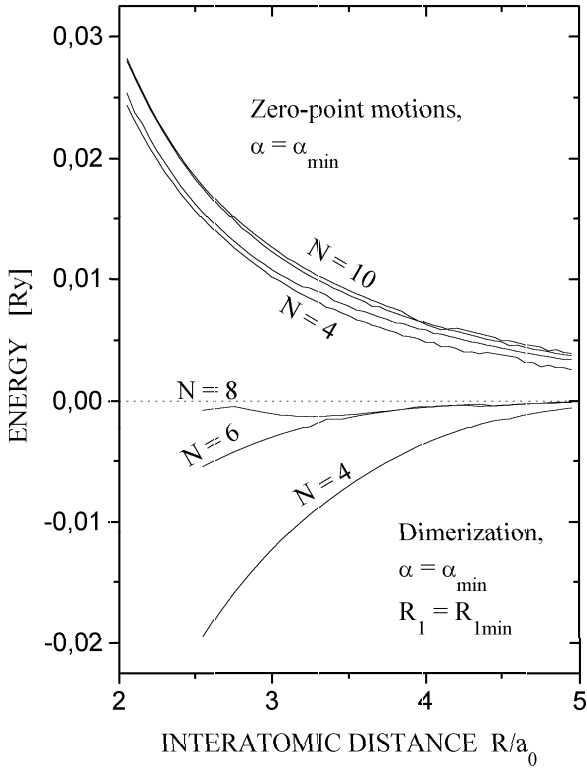


FIG. 14. Ground-state-energy changes due to the dimerization (bottom panel) and to the zero-point motion (top panel), plotted for different  $N$ , as a function of  $R$ .

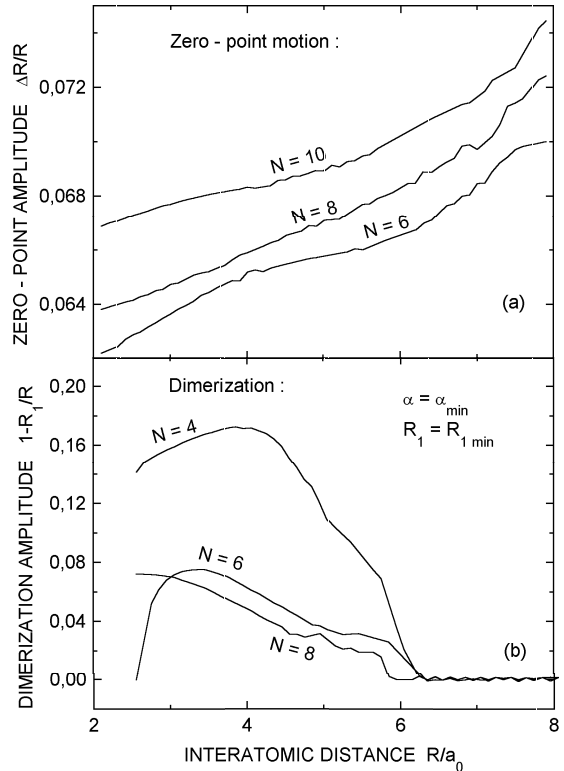


FIG. 15. Atomic shift due to the dimerization and the root-mean-square amplitude of the zero point motion vs.  $R$  and for different  $N$  (top and bottom parts, respectively).

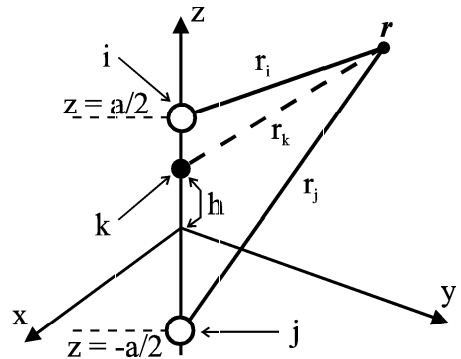


FIG. 16. Configuration of coordinates used to calculate the three-site terms in the hopping integral  $t'_{ij}$  for the electron transfer  $j \rightarrow i$  induced by the Coulomb potential of  $k$ -th ion.